UNIVERSITY OF FLORIDA

DETERMINATION OF ELECTROCHEMICAL PERFORMANCE, AND THERMO-MECHANICAL-CHEMICAL STABILITY OF SOFCS FROM DEFECT MODELING

Eric D. Wachsman, Keith L. Duncan and Fereshteh Ebrahimi
Department of Materials Science
University of Florida, Gainesville FL 32611

Department of Energy, Contract Number DE-FC26-02NT41562

Yanli Wang, Jeremiah Smith, Mark Clarke, Aiijie Chen, Sean Bishop

OBJECTIVES

1. Provide fundamental relationships between SOFC performance and operating conditions (T, P_{O_2}, V, etc..)
2. Transient (time dependent) transport properties
3. Extend models to:
   - Thermo-mechanical stability
     - Thermal and thermochemical expansion
     - Elastic modulus
     - Fracture toughness
   - Thermo-chemical stability
     - Pore formation and reactions at cathode/electrolyte interface
   - Multilayer structures
     - Interfacial defect concentration, etc.
4. Incorporate microstructural effects such as grain boundaries and grain-size distribution
5. Experimentally verify models and devise strategies to obtain relevant material constants
6. Assemble software package for integration into SECA failure analysis models

Features of the Defect Model

- Continuous functions for the defect concentrations vs. discontinuous "piecewise" Brouwer approach.
- Dependent on thermodynamic quantities, namely the mass-action constants (K's).
- Quantitative for any SOE/MIEC.
- Derived from fundamental thermodynamic equations.

Electron-Hole Pair Formation

$$null \leftrightarrow e' + h^{\bullet}$$

$$K_i = c_e c_h = N_v N_c \exp\left(-E_g / k_B T\right)$$

External Equilibria

$$O_O^{\times} \leftrightarrow V_O^{\bullet\bullet} + 2e' + \tfrac{1}{2} O_2$$

$$K_r = c_V c_e^2 P_{O_2}^{\frac{1}{2}} = K_r^* \exp\left(-\Delta G_r / k_B T\right)$$

Internal Equilibria

$$O_O^{\times} \leftrightarrow V_O^{\bullet\bullet} + O_i''$$

$$K_f = c_V c_I$$

Defect Triads (CLEM) vs. Defect Pairs (Brouwer)

$$c_e + c_A = 2c_V$$

Limiting Case

$$P_{O_2} >> 4^{-4} K_r^2 c_V^{-6}$$

$c_e = 2c_V$ …Region I

$c_A = 2c_V$ …Region IIa

CONTINUUM LEVEL ELECTROCHEMICAL MODEL
Defect Equilibria

MODEL

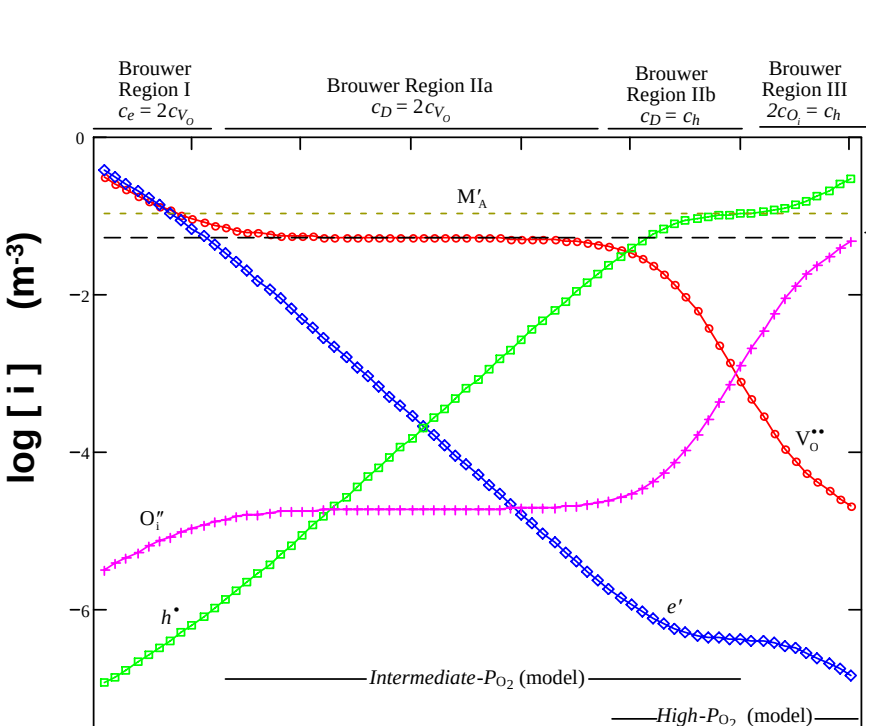

BROUWER APPROACH

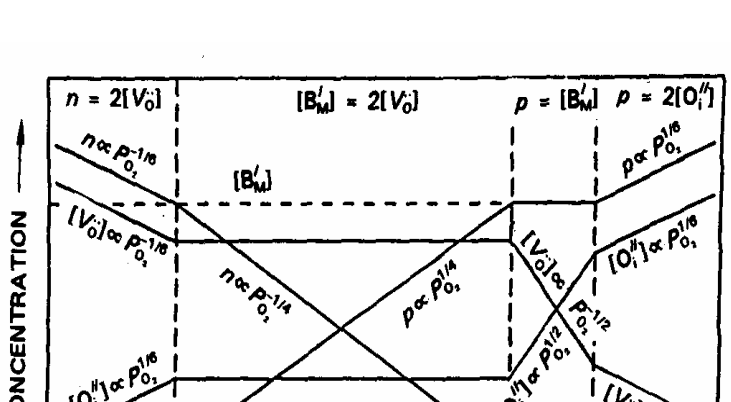

Variation of defect concentration as a function of oxygen partial pressure for MO_2-B_2O_3 system [3.17]

Verified experimentally
- vs. other models[1]
- vs. conductivity[2]
- vs. OCP

1. O. Porat and H. L. Tuller, *J. Electroceramics* **1** (1997) 42; 2. Eguchi et al, *Solid State Ionics* **52** (1992) 265.

CONTINUUM LEVEL ELECTROCHEMICAL MODEL
Defect Equilibria

FLUORITE

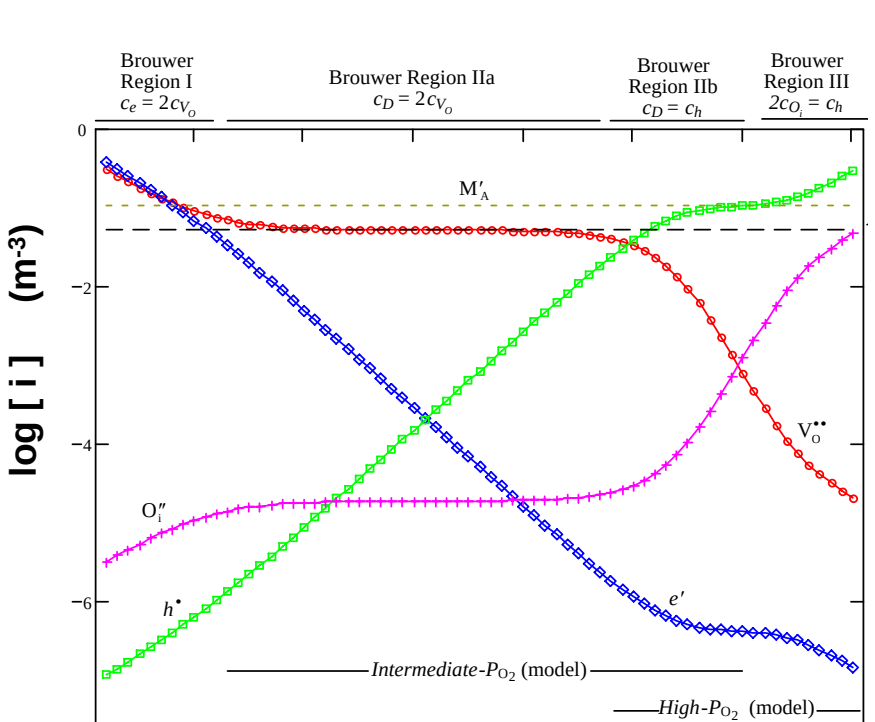

PEROVSKITE

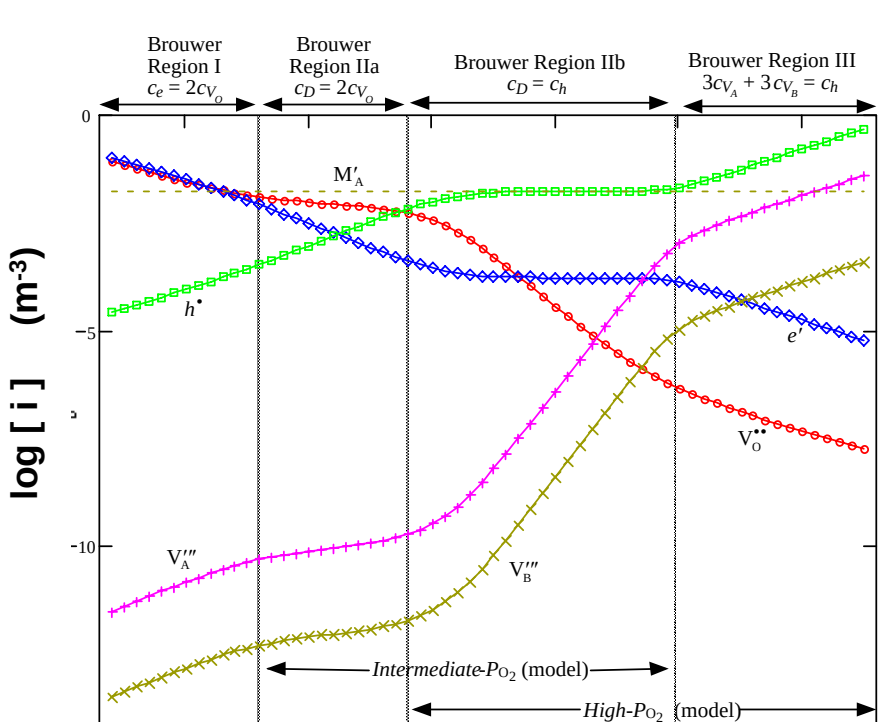

Verified experimentally
- vs. other models[1]
- vs. conductivity[2]
- vs. OCP

Universal to all materials

1. O. Porat and H. L. Tuller, *J. Electroceramics* **1** (1997) 42; 2. Eguchi et al, *Solid State Ionics* **52** (1992) 265.

FUNDAMENTAL TRANSPORT EQUATIONS & DEFINITIONS

j	flux
J	current
c	concentration
ϕ	potential
z	charge num.
q	elec. charge
σ	conductivity
u	mobility
D	diffusivity
L	thickness
k_B	Boltz. const.
Φ_{th}	Nernst poten.
Φ_{app}	exter. potential
T	temperature

Subscripts

V	O_2 vacancies
e	electrons

Nernst-Planck $$j_i = -D_i \nabla c_i - u_i c_i \nabla \phi$$

Current $$J = \sum_i J_i = q \sum_i z_i j_i$$

Average conductivity $$\overline{\sigma}_i^{-1} = L^{-1} \int_0^L \left[\sigma_i(x)\right]^{-1} \cdot \mathrm{d}x$$

Charge neutrality $$\sum_i z_i c_i = z_V c_V + z_A c_A + z_e c_e \approx 0$$

Local equilibrium

$$\phi_L - \phi_0 = \Delta\phi = \Phi_{app} - \Phi_{th} - k_B T \left(z_V q\right)^{-1} \ln\left(c_{V_L} / c_{V_0}\right)$$

NON-LINEAR POTENTIAL MODEL
Potential Distribution

$\nabla J = 0$ & $\nabla j_i = 0$

$$\nabla^2\phi = \lambda\nabla^2 c_V$$

$$\frac{\left(z_V u_e j_V - u_V j_e\right)c_V - j_V u_e c_A}{z_V\left(z_V - z_e\right)c_V - c_A} = \frac{qD_e D_V}{k_B T}\nabla c_V$$

$$c_V(x) - c_{V_0} - \frac{\phi(x) - \phi_0}{\lambda} = -\gamma x$$

$$c_V(x) - c_{V_0} - \frac{\left(D_V\gamma - j_V\right)c_A}{z_V\left(z_V - z_e\right)D_V\gamma}\cdot\ln\frac{z_V\left(z_V - z_e\right)D_V\gamma c_V(x) - j_V c_A}{z_V\left(z_V - z_e\right)D_V\gamma c_{V_0} - j_V c_A} = -\gamma x$$

$$\phi(x) = \phi_0 - \frac{\left(D_V\gamma - j_V\right)k_B T}{z_V q D_V\gamma}\cdot\ln\frac{z_V\left(z_V - z_e\right)D_V\gamma c_V(x) - j_V c_A}{z_V\left(z_V - z_e\right)D_V\gamma c_{V_0} - j_V c_A}$$

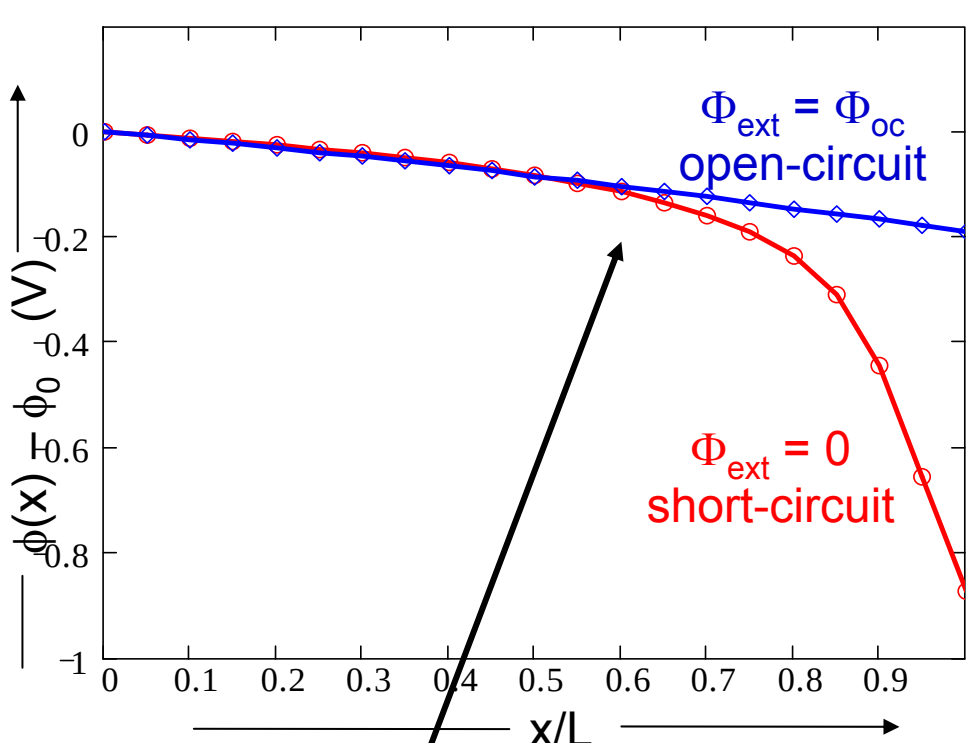

Solved the fundamental transport equations under both:

- Linear potential model (LPM) - Laplace potential distribution
- Non-linear potential model (N-LPM) - Poisson potential distribution

NON-LINEAR POTENTIAL MODEL

Defect Concentration Profiles, Transference Number, and Cell Efficiency

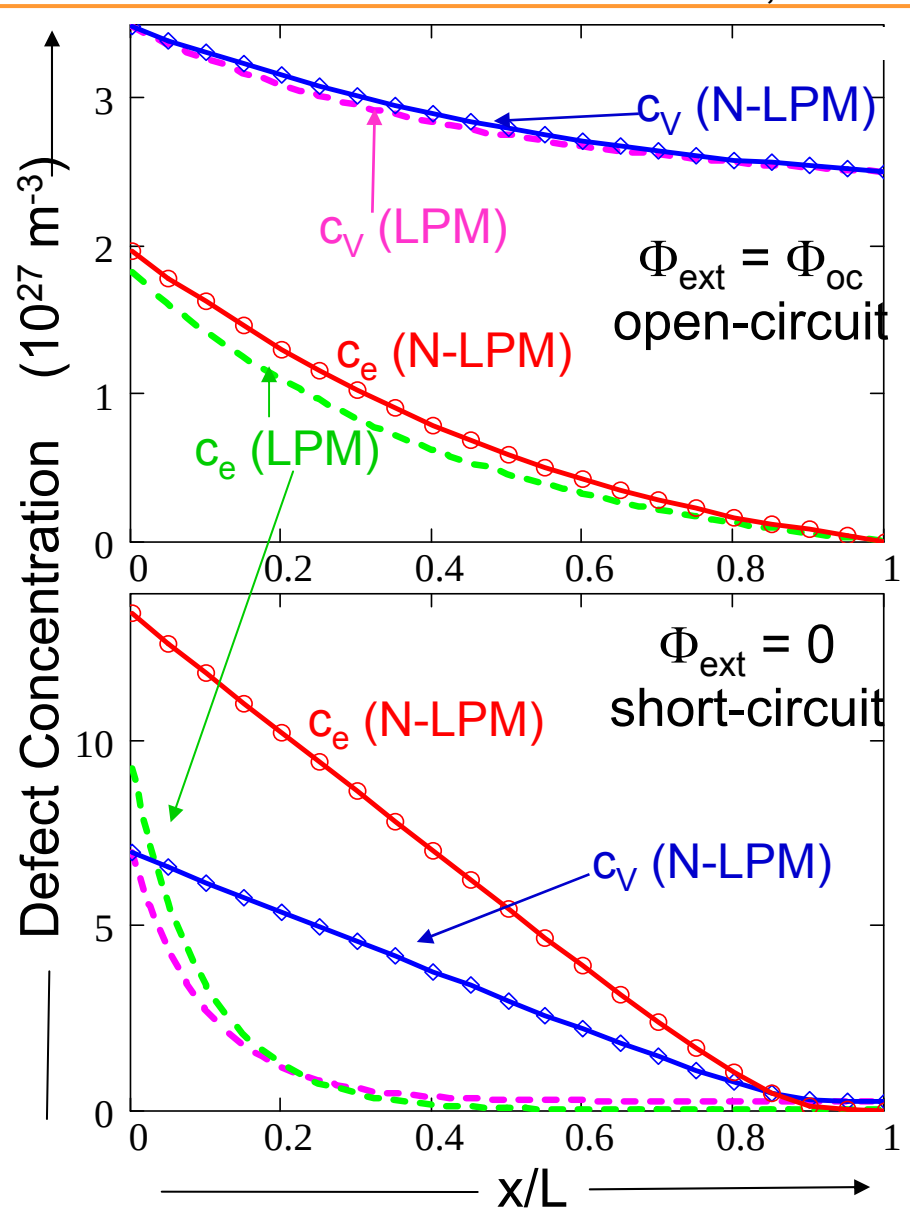

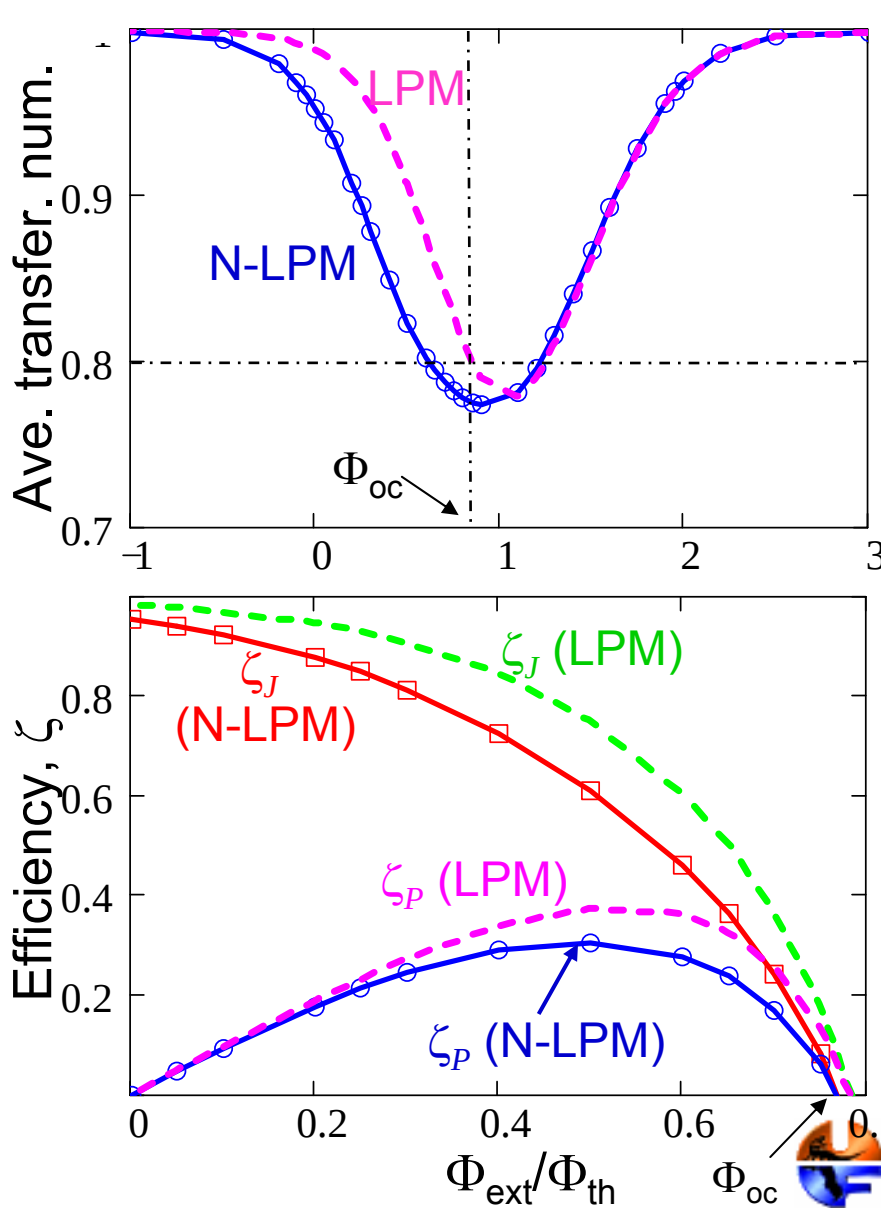

CONTINUUM LEVEL ELECTROCHEMICAL MODEL

Transient Effects

$R \equiv f(P_{O_2}, c_i, \Phi_{ext}, K)$

$C \equiv f(P_{O_2}, c_i, \Phi_{ext}, K)$

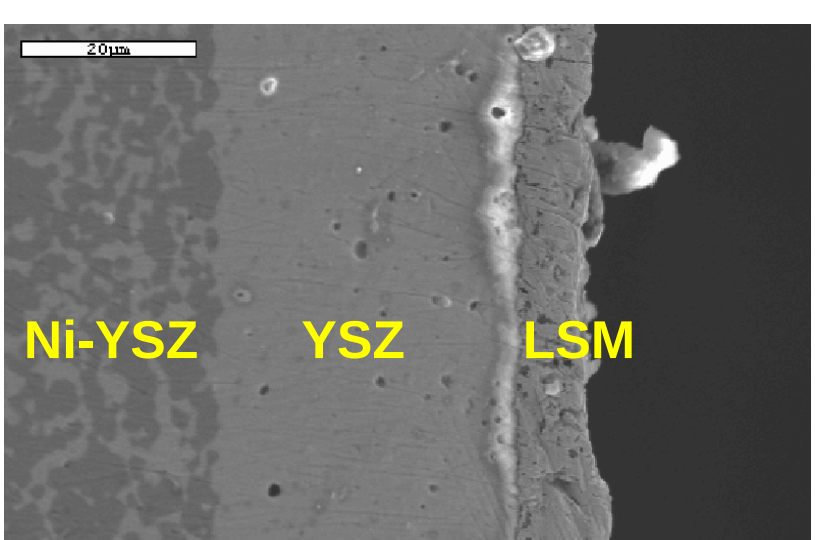

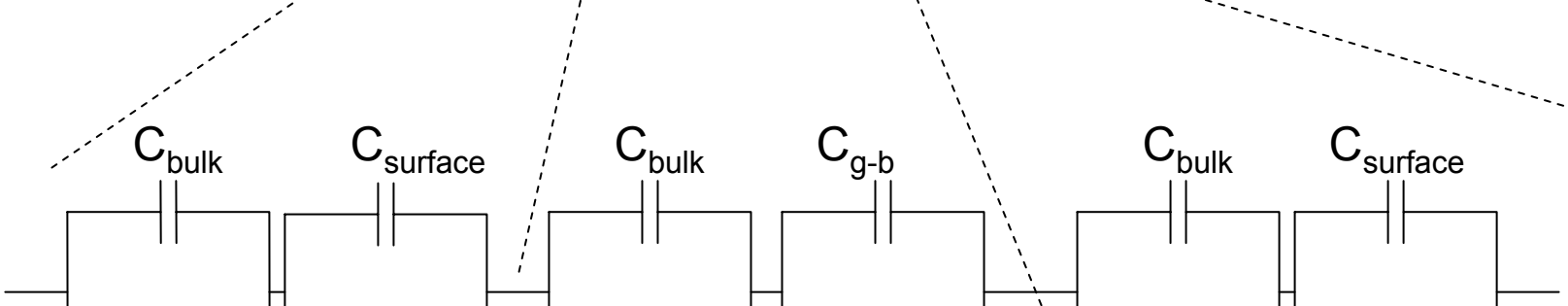

CONTINUUM LEVEL ELECTROCHEMICAL MODEL

Transient Effects

Nernst-Planck flux equation

$$j_i = -D_i \nabla c_i - u_i c_i \nabla \phi$$

Material balance equation

$$\frac{\partial c_i}{\partial t} = -\nabla j_i$$

Current equation

$$J = q \sum_i z_i j_i$$

Equations for flux, material balance, current and charge neutrality are manipulated to obtain expressions for the rate of change of defect concentration.

$$\frac{\partial c_V}{\partial t} = \frac{D_e D_V}{z_e D_e - z_V D_V} \left[(z_e - z_V) \nabla^2 c_V + z_e c_A \frac{q}{k_B T} \nabla^2 \phi \right]$$

$$\frac{\partial c_e}{\partial t} = \frac{D_e D_V}{z_e D_e - z_V D_V} \left[(z_e - z_V) \nabla^2 c_e + z_e z_V c_A \frac{q}{k_B T} \nabla^2 \phi \right]$$

And an expression for the electric field as a function of defect concentrations.

$$\nabla \phi = -\frac{J + \left(z_V q D_V \nabla c_V + z_e q D_e \nabla c_e \right)}{q \left(z_V u_V c_V + z_e u_e c_e \right)}$$

CONTINUUM LEVEL ELECTROCHEMICAL MODEL

Transient Effects

Introduction of a P_{O_2} gradient

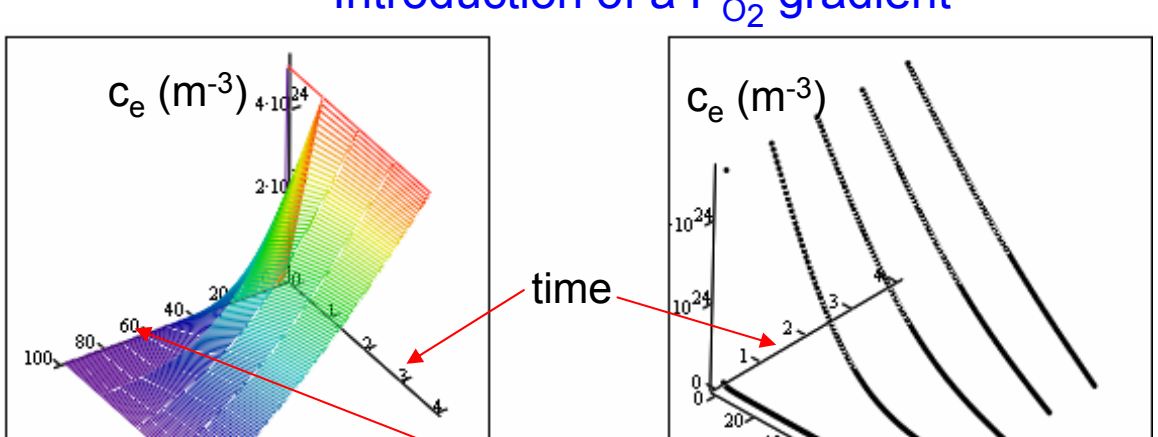

Introduction of a P_{O_2} gradient and a sinusoidal perturbation

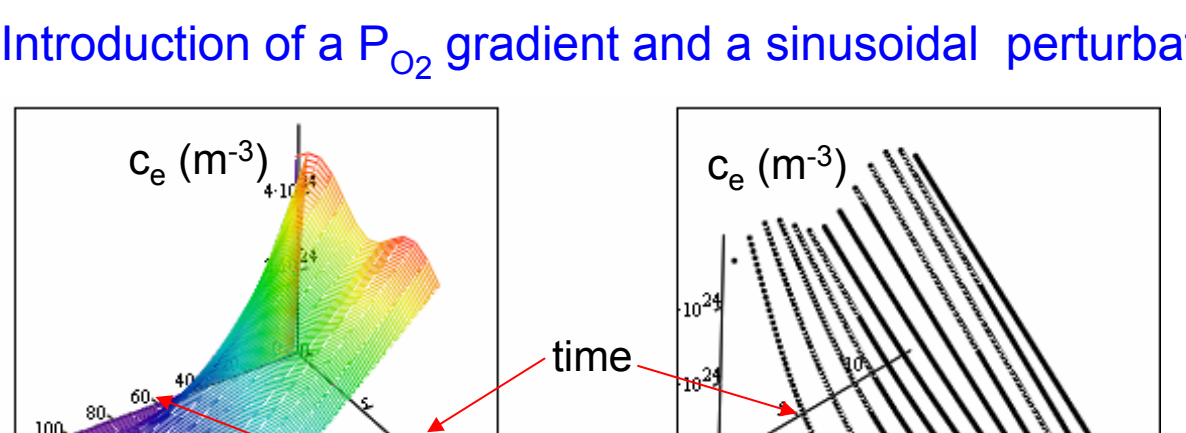

CONTINUUM LEVEL ELECTROCHEMICAL MODEL
Transient Effects

Case 2 Changing the P_{O_2} gradient/applied potential/load resistance

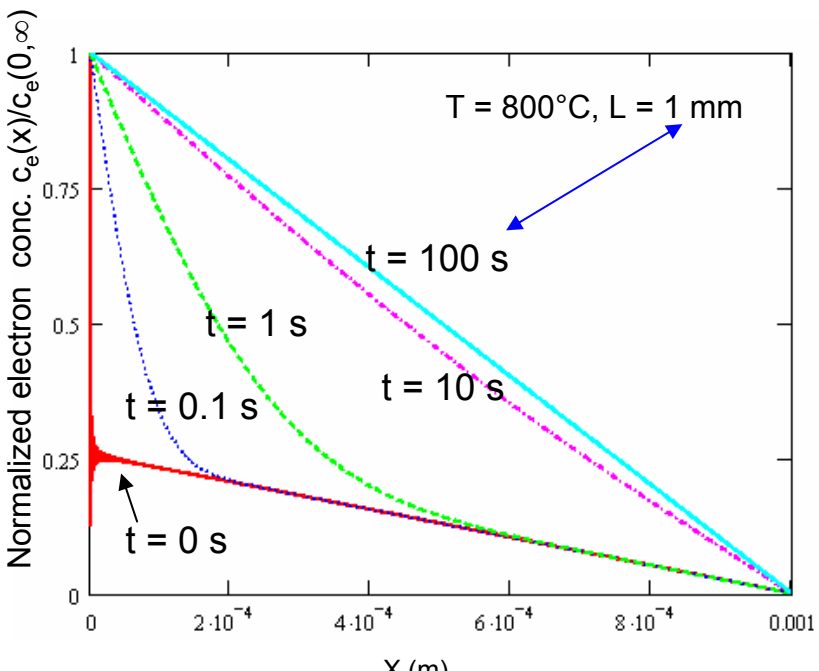

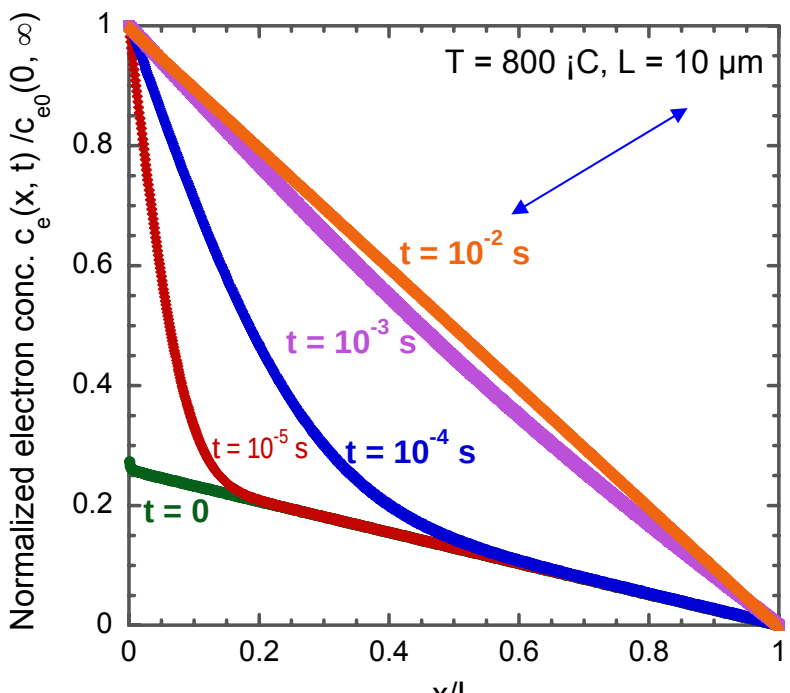

Importance of transients depends on layer thickness

For the above processes, the time constant, τ,

- $\tau \propto 1/L$ (steady-state achieved more rapidly for thinner electrolytes)
- $\tau \propto D_e$ (rapid electron diffusion helps system to reach steady-state

TASKS TO BE PERFORMED IN PHASE II

1. Extend Continuum-Level Electrochemical Model to Include Multi-Layer Structures

Determine effects of component thickness ratios and operating conditions on the concentration of defect species and oxygen potential at component interfaces.

2. Extend Continuum-Level Electrochemical Model to Include Microstructural Effects

Determine effects of microstructure on the electrical, thermo-mechanical and thermo-chemical stability of SOFC components and SOFC performance.

3. Experimentally Verify Electrochemical Performance, Chemical Stability, & Transient Aspects of Model

Obtain frequency dependent impedance and electrode overpotential data from electrochemical measurements (ac impedance spectroscopy, potentiometric, current interrupt, etc,) to determine effects of porosity and pore diffusion (electrodes); grain boundaries (electrolyte); and grain-size distribution.

Induce degradation/failure in cathode/electrolyte bilayers by thermal cycling, high temperature sintering and DC bias to initiate tertiary phase formation or delamination at the interface. Experimentally determine cell time constants from R-C circuit analysis and use in evaluating the effect of voltage transients from the power conditioning equipment on failure mechanisms.

4. Experimentally Verify Thermo-Mechanical Model

Measure oxygen stoichiometry (Cahn Microbalance) and material expansion (Theta Dilatometer) as a function of P_{O_2} & T. Measure modulus and fracture toughness of single crystal regions as a function of P_{O_2} & T (Triboindenter). Measure modulus and fracture toughness of polycrystalline samples (MTS system) and separate bulk property vs. microstructural effects. Compare with data obtained at ORNL.

5. Package and Deliver Software

Develop software modules of the models for use by NETL, PNNL, ORNL and SECA industrial teams.

EXTEND ELECTROCHEMICAL MODEL TO MULTILAYER STRUCTURES
Thermochemical Stability of Electrolyte/Cathode Interface

$$La_{1-y}Sr_yMnO_{3-\delta} + \delta ZrO_2 + \frac{3\delta}{2} O_O^{\times} \rightarrow La_{1-y-\delta}Sr_yMnO_{3-\delta} + \frac{\delta}{2} La_2Zr_2O_7 + \frac{3\delta}{2} V_O^{\bullet\bullet} + 3\delta e'$$

$$K \approx \left[La_2Zr_2O_7\right]^{\frac{\delta}{2}} \left[V_O^{\bullet\bullet}\right]^{\frac{3\delta}{2}} \left[e'\right]^{3\delta} = K_2 \left[La_2Zr_2O_7\right]^{\frac{\delta}{2}} P_{O_2}^{-\frac{3\delta}{4}}$$

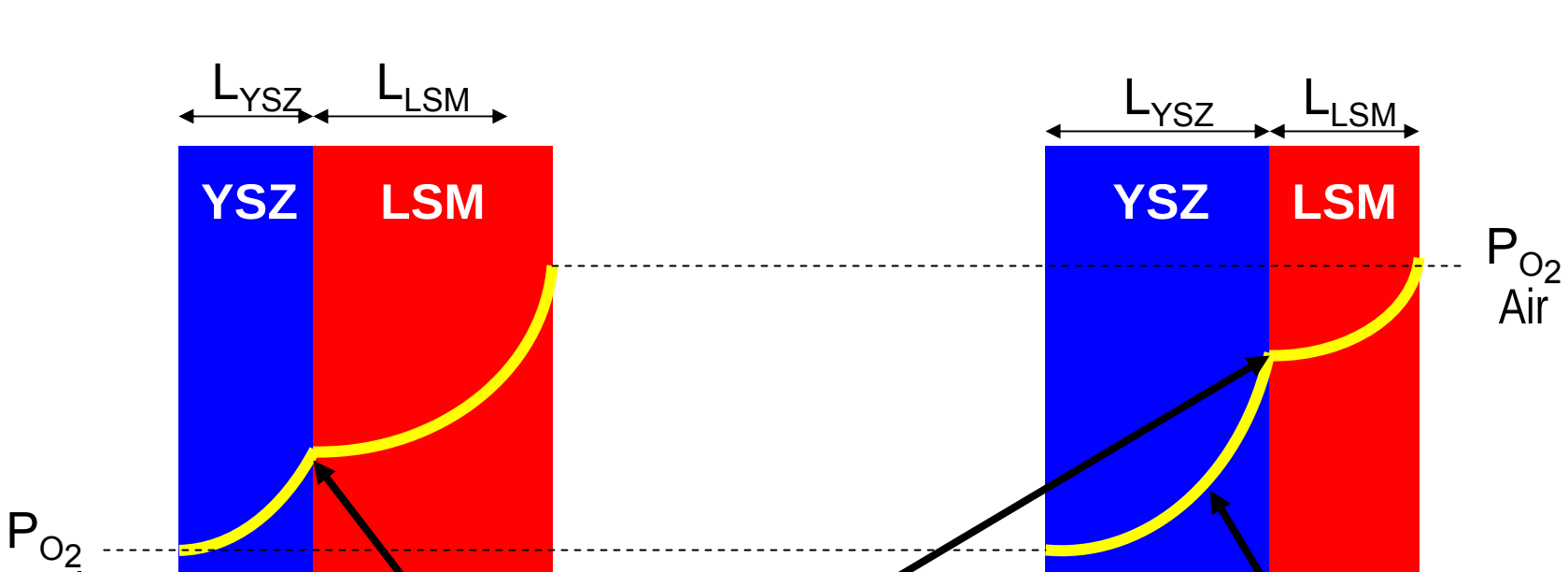

EXTEND ELECTROCHEMICAL MODEL TO MULTILAYER STRUCTURES
Thermochemical Stability of Electrolyte/Cathode Interface

Thickness ratio (L_{LSM}/L_{YSZ})

QuickTime™ and a
TIFF (LZW) decompressor
are needed to see this picture.

H_2/H_2O at the anode; air at the cathode
open-circuit voltage, V_{oc} ~ 1.1 V @ 800 °C
max power @ $V_{cell} \approx V_{oc}/2$
short-circuit @ $V_{cell} \approx 0$

Voltage drop across LSM (V)

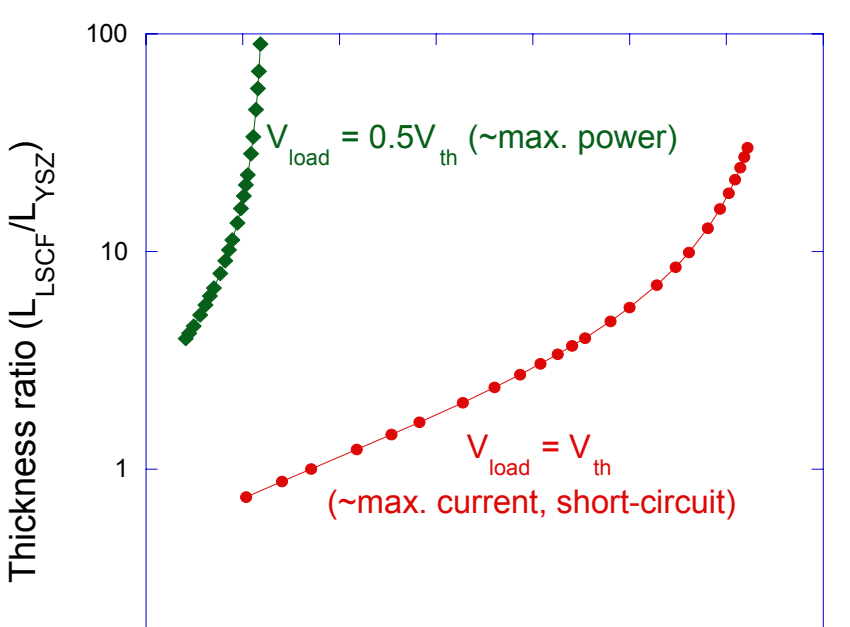

LSM/YSZ and LSCF bilayers were modeled using a dense LSM or LSCF layer:

- This ***does not*** allow for vacancy transport or a significant P_{O2} gradient in the **LSM** layer.
- This ***does*** allow for vacancy transport resulting in a significant P_{O2} gradient in the **LSCF** layer.
- The observed trends are reasonable since the voltage drop across the LSM and LSCF layers increase with relative thickness.
- More appropriate microstructure will be included in the next iteration of the model.

EXTEND MODEL TO INCLUDE MICROSTRUCTURAL EFFECTS
Concentration Overpotential

CATHODE

$$P_{O_2,\text{cathode-electrolyte interface}} = P_{\text{atmos}} - \left(P_{\text{atmos}} - P_{O_2@\text{air}}\right)\exp\left(\frac{kT}{4q}\cdot\frac{\tau_c}{D_c}\cdot\frac{L_c}{\varepsilon_c}\cdot J\right)$$

tortuosity

gas diffusivity

porosity

ANODE

$$P_{H_2,\text{anode-electrolyte interface}} = P_{H_2@\text{fuel}} - \frac{kT}{2q}\cdot\frac{\tau_a}{D_a}\cdot\frac{L_a}{\varepsilon_a}\cdot J$$

$$P_{H_2O,\text{anode-electrolyte interface}} = P_{H_2O@\text{fuel}} + \frac{kT}{2q}\cdot\frac{\tau_a}{D_a}\cdot\frac{L_a}{\varepsilon_a}\cdot J$$

J.-W. Kim, A. Virkar, K.-Z. Fung, K. Mehta and S. Singhal, *J. Electrochem. Soc.*, **146** (1999) 69-78

S. Chan, K. Khor, Z. Xia, *J. Power Sources*, **93** (2001) 130

DEFECT CONCENTRATION

$$K\big|_{J=0}\exp\left(\frac{q\eta}{kT}\right) = \frac{c_V c_e^2}{1-c_V}P_{O_2}^{\frac{1}{2}}$$

ACTIVATION OVERPOTENTIAL

$$J = J_0\left[\exp\left(\frac{q}{kT}\alpha\eta\right) - \exp\left(-\frac{q}{kT}(1-\alpha)\eta\right)\right]$$

POTENTIAL

$$\Phi_{ext} - \Phi_{th} - \frac{k_B T}{z_V q}\ln\frac{c_{V_L}}{c_{V_0}} = \frac{z_V u_e + u_V\left(1-\dfrac{\eta}{\Phi_{th}-\Phi_{ext}}\right)}{u_e - u_V\left(1-\dfrac{\eta}{\Phi_{th}-\Phi_{ext}}\right)}\cdot\frac{k_B T}{z_V q}\ln\frac{c_{V_L} - \dfrac{u_e c_A / z_V}{u_e - u_V\left(1-\dfrac{\eta}{\Phi_{th}-\Phi_{ext}}\right)}}{c_{V_0} - \dfrac{u_e c_A / z_V}{u_e - u_V\left(1-\dfrac{\eta}{\Phi_{th}-\Phi_{ext}}\right)}}$$

EXTEND MODEL TO INCLUDE MICROSTRUCTURAL EFFECTS

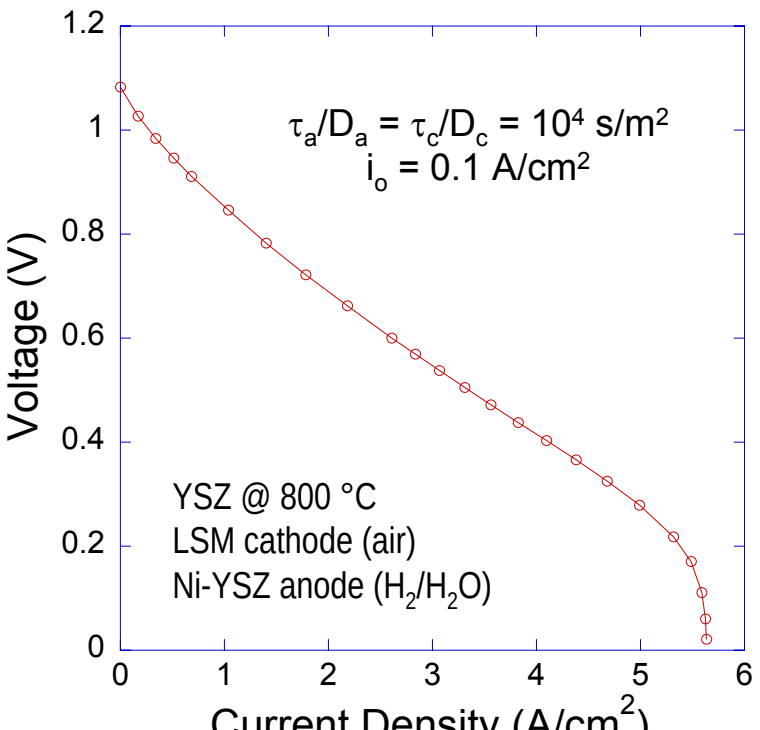

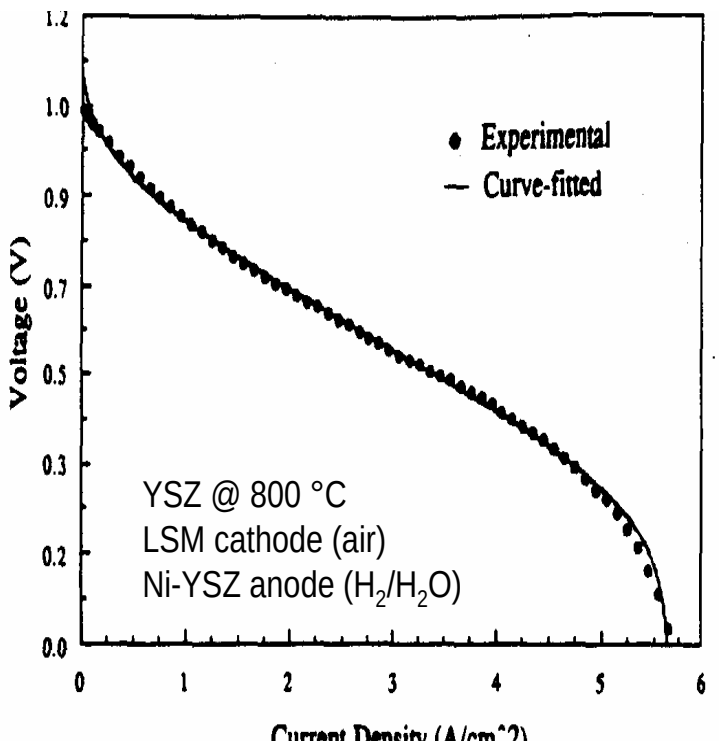

Figure 5. Experimental data at 800°C and the corresponding best fit to Eq. 45.

- Electrochemical model (with pore diffusion incorporated) matches "Virkar"* model, but with less fitting parameters, (3 vs. 10)
- Fitting parameters: τ_a/D_a (effective tortuosity anode), τ_c/D_c (effective tortuosity cathode) and i_o (exchange current density).

*J.-W. Kim, A. Virkar, K.-Z. Fung, K. Mehta and S. Singhal, *J. Electrochem. Soc.*, **146** (1999) 69-78

EXTEND MODEL TO INCLUDE MICROSTRUCTURAL EFFECTS

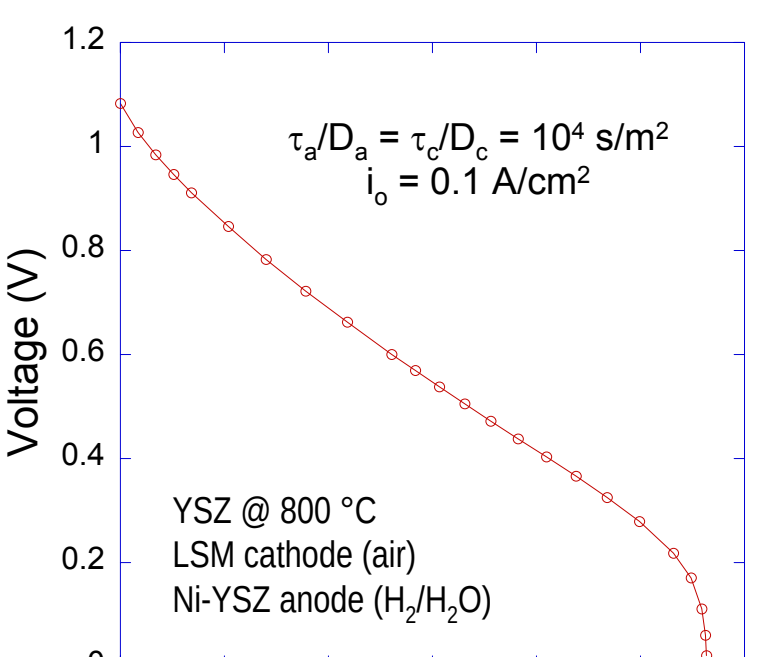

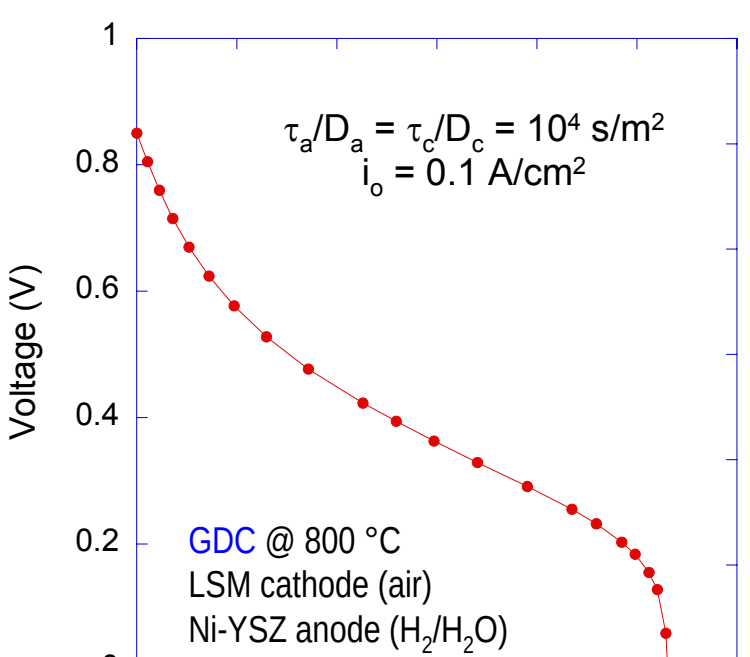

I-V & power density curves can also be generated for mixed conducting materials:

- Electrolytes such as GDC (above)
  - -Shows reduction in OCP and current density due to low t_i at 800°C
- Cathodes such as LSF and LSCF (near future)

EXTEND MODEL TO INCLUDE MICROSTRUCTURAL EFFECTS

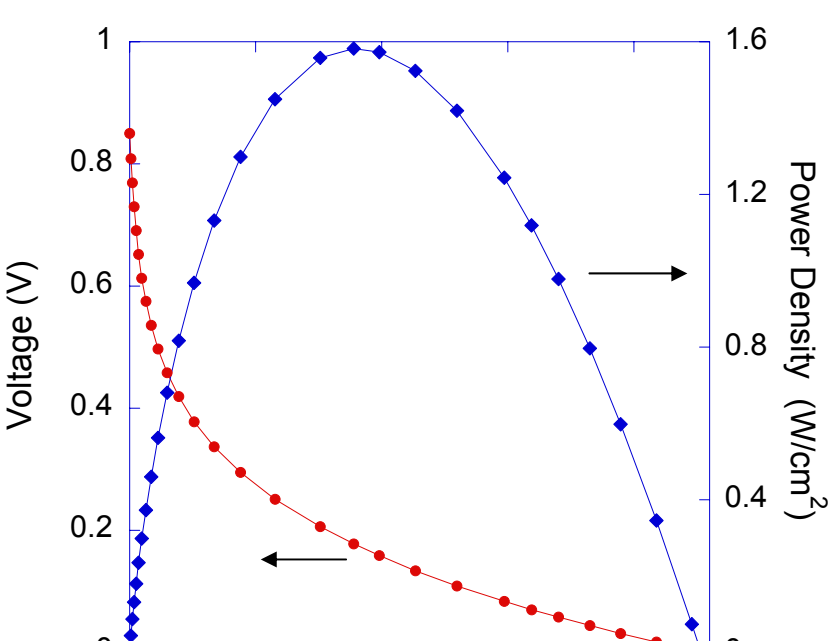

$\tau_a/D_a = \tau_c/D_c = 10^2$ s/m^2
$i_o = 0.1$ A/cm^2

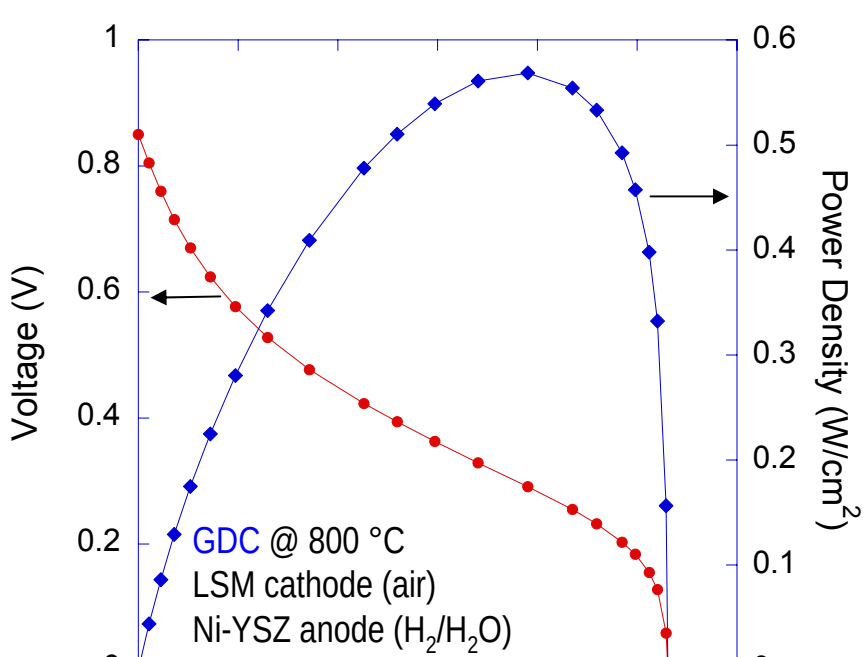

$\tau_a/D_a = \tau_c/D_c = 10^4$ s/m^2
$i_o = 0.1$ A/cm^2

Model shows decrease in effective tortuosity (τ/D) can dramatically increases power density

VERIFY ELECTROCHEMICAL PERFORMANCE ASPECTS OF MODEL

- Prepare different microstructures
  - -LSM,LSF, and LSCF (powders supplied by NexTech)
  - -Sintering temperature and time
  - -Pore former
- Measure electrochemical performance and compare with model

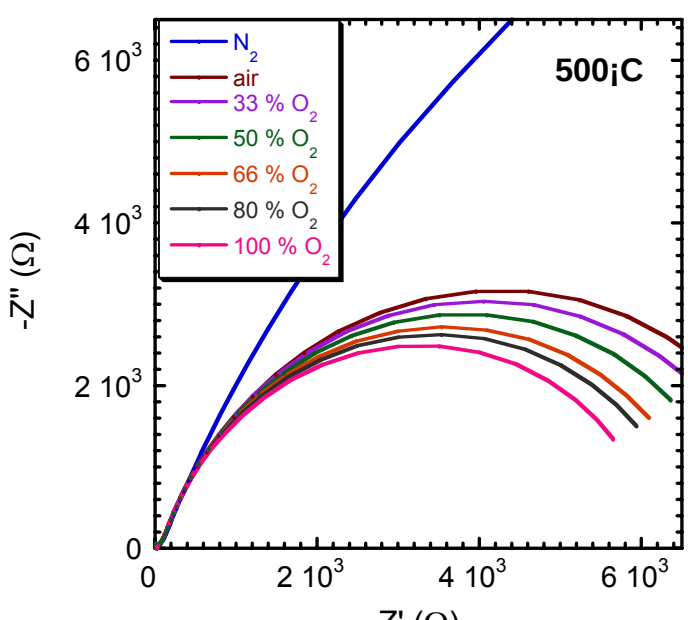

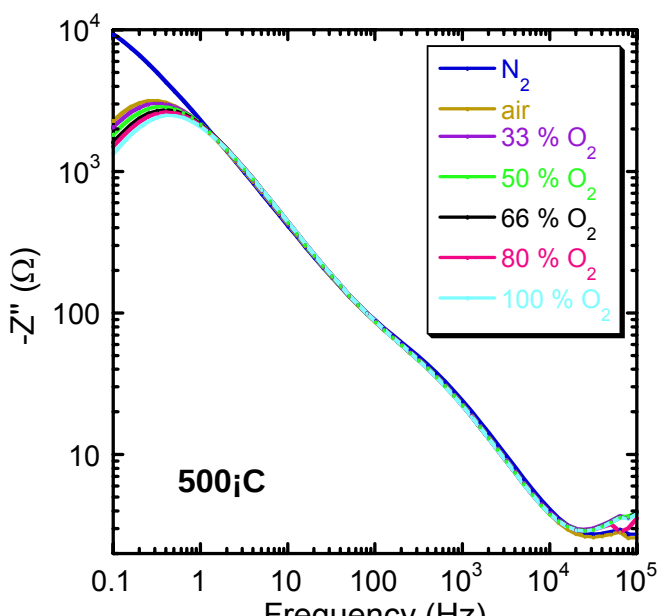

Effect of P_{O2} on AC Impedance Spectra of LSM/YSZ/LSM Cells

- As P_{O2} decreases the impedance of low frequency arc increases indicating gas diffusion limited - *concentration overpotential*

VERIFY ELECTROCHEMICAL PERFORMANCE ASPECTS OF MODEL

Microstructure/Impedance - LSM Sintering Time Effect

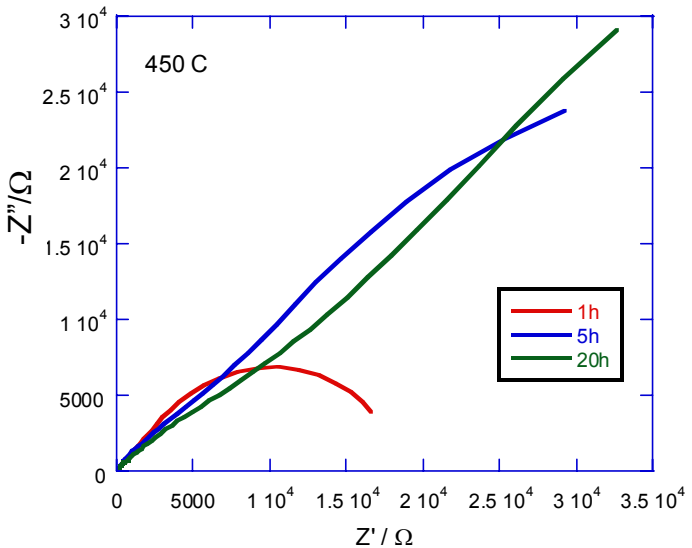

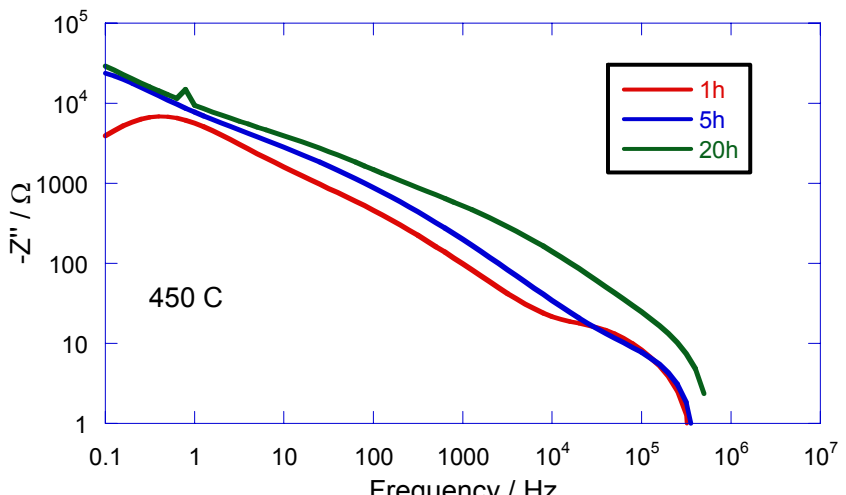

1100 °C 1h

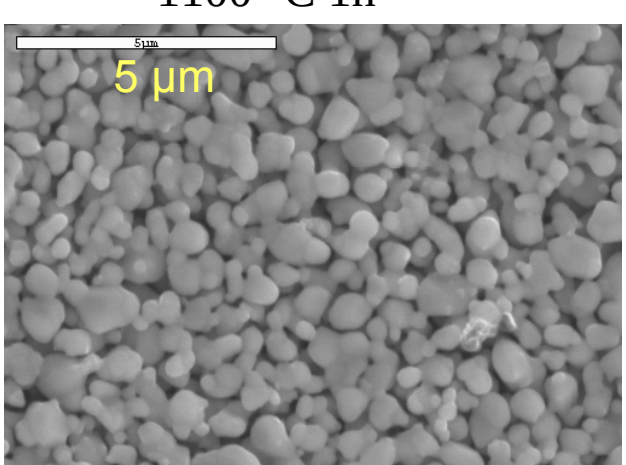

1100 °C 20h

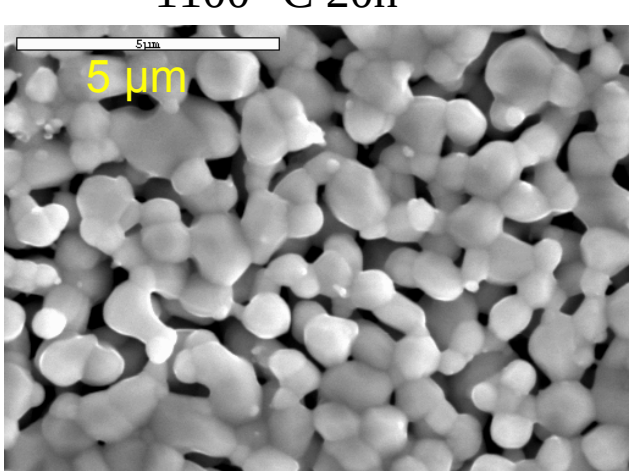

Long anneal coarsens electrode microstructure increasing low frequency impedance

Powder supplied by NexTech

VERIFY ELECTROCHEMICAL PERFORMANCE ASPECTS OF MODEL

Microstructure/Impedance - LSCF Sintering Time Effect

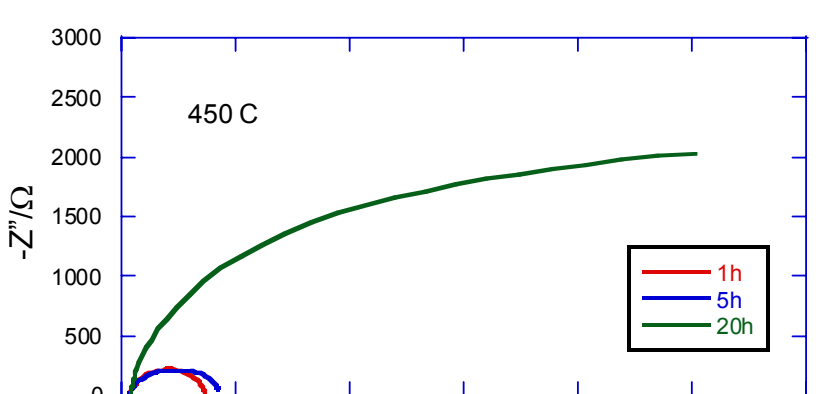

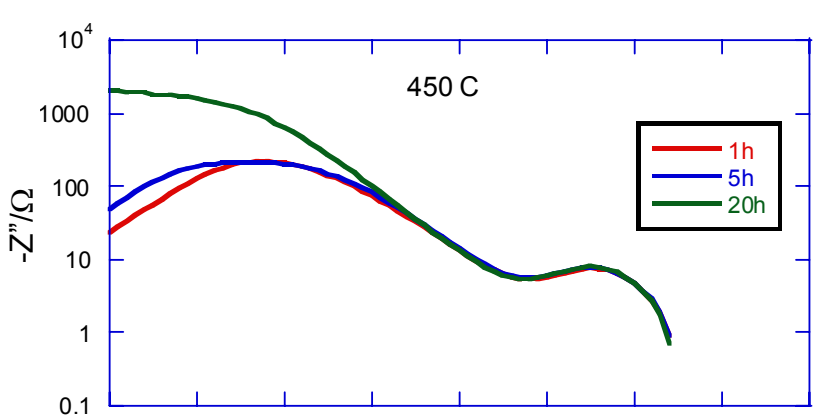

950 °C 1h

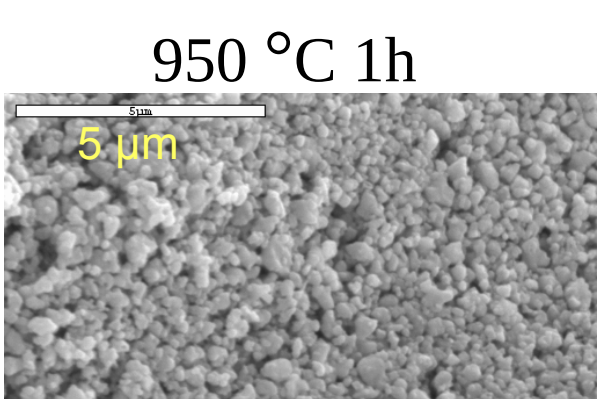

950 °C 20h

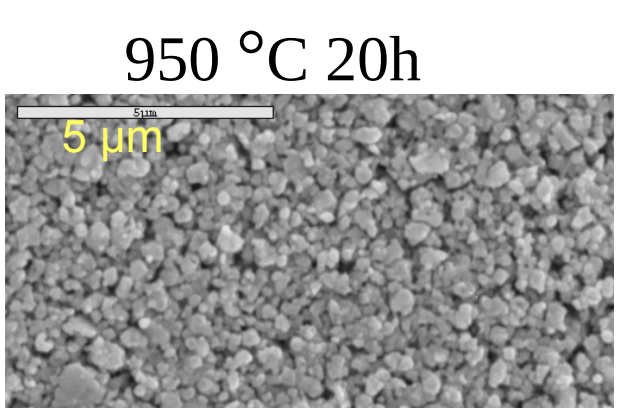

Long anneal increases low frequency impedance

Powder supplied by NexTech

VERIFY ELECTROCHEMICAL PERFORMANCE ASPECTS OF MODEL

Microstructure/Impedance - LSF Sintering Time Effect

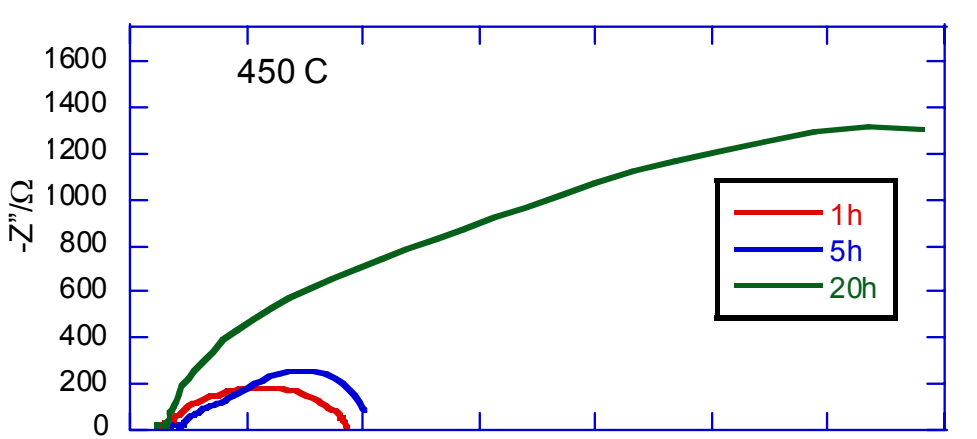

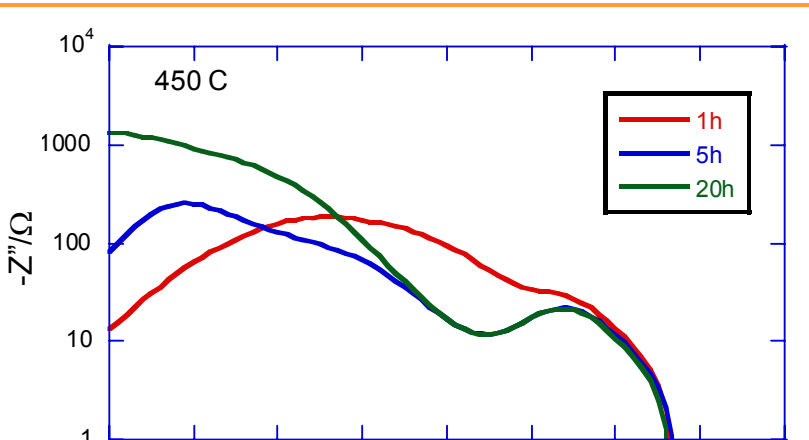

950 °C 1h

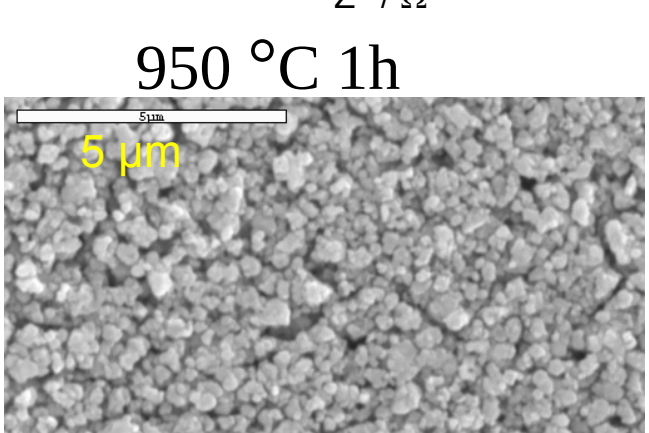

950 °C 20h

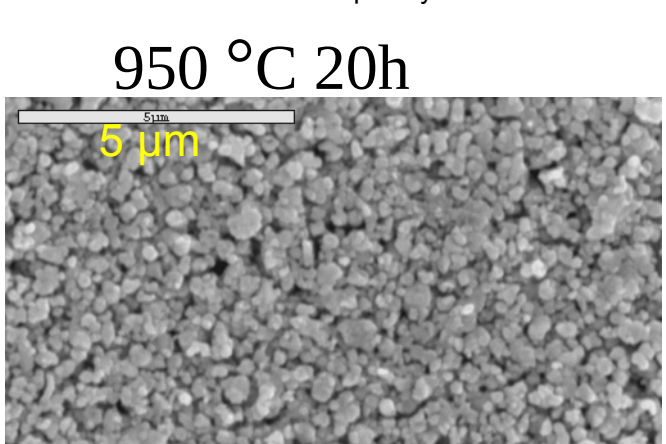

Long anneal increases low frequency impedance

Powder supplied by NexTech

VERIFY ELECTROCHEMICAL PERFORMANCE ASPECTS OF MODEL

Microstructure/Impedance - LSM Sintering Temperature Effect

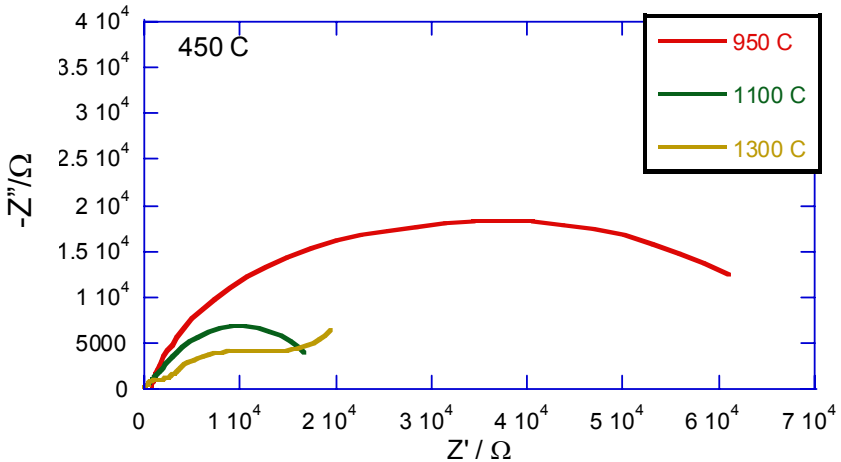

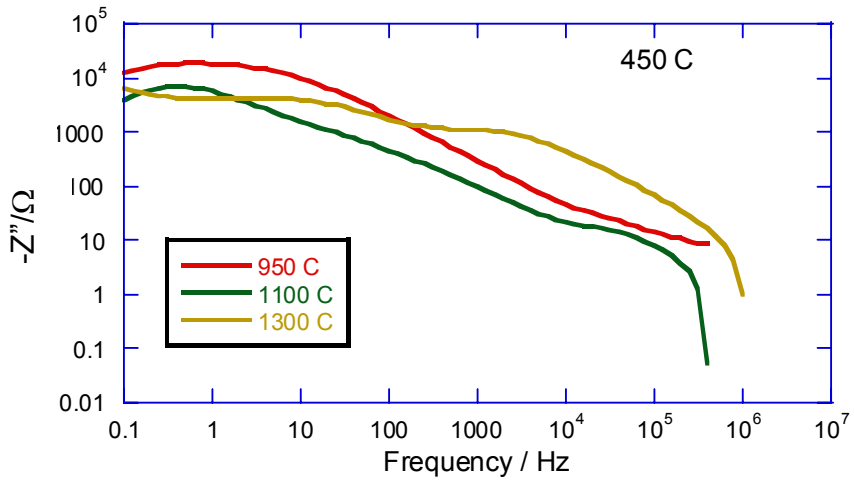

950 °C

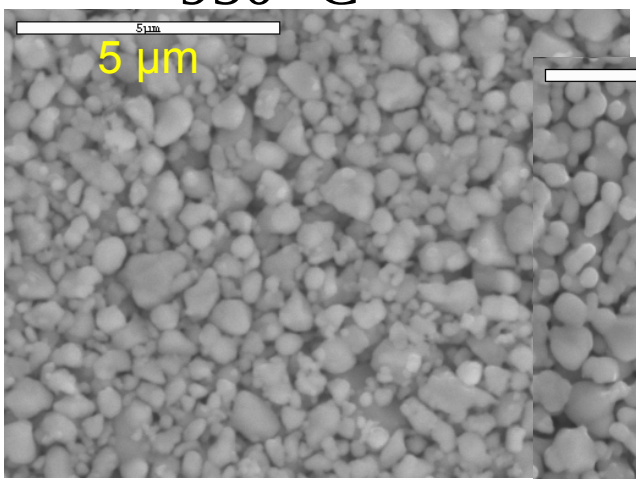

1100 °C

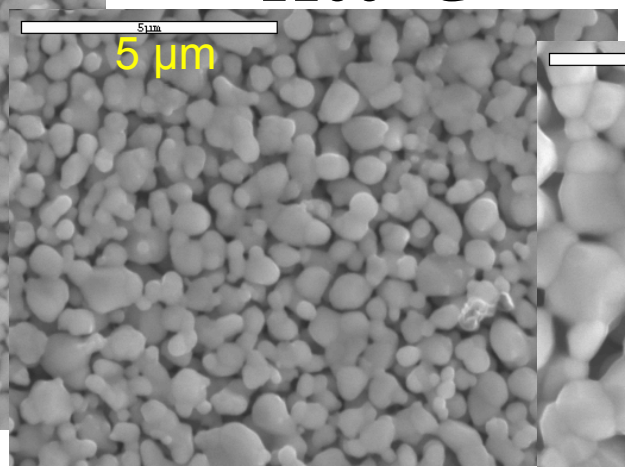

1300 °C

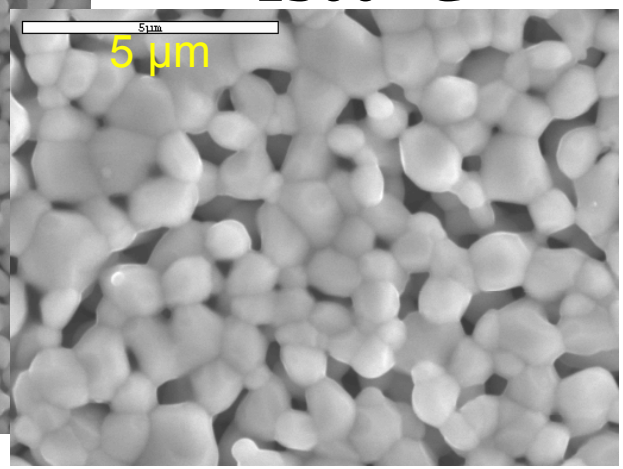

Higher temperature coarsens microstructure - multiple changes to impedance

Powder supplied by NexTech

VERIFY ELECTROCHEMICAL PERFORMANCE ASPECTS OF MODEL

Microstructure/Impedance - LSCF Sintering Temperature Effect

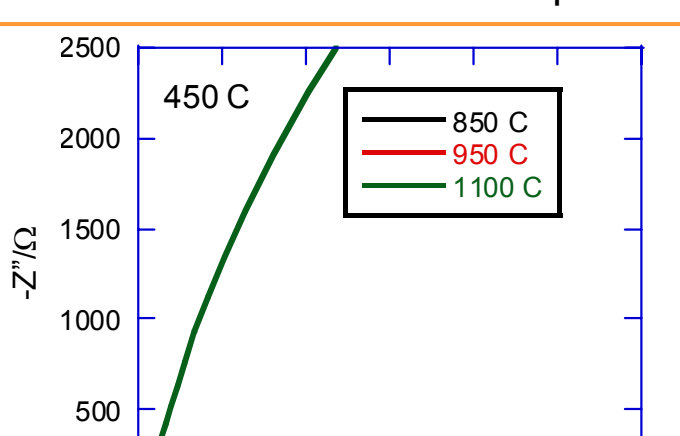

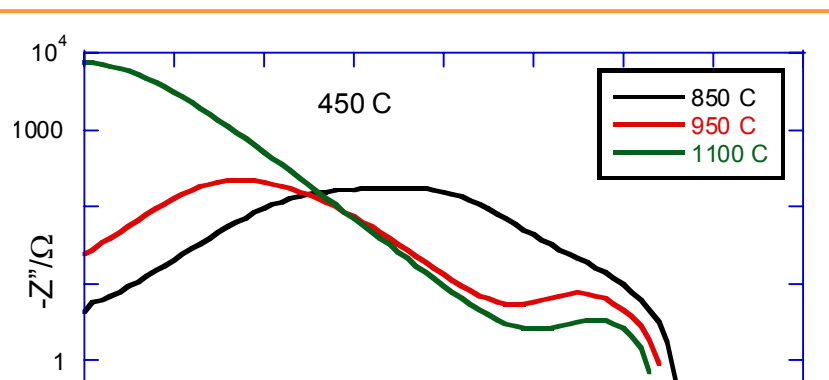

850 °C

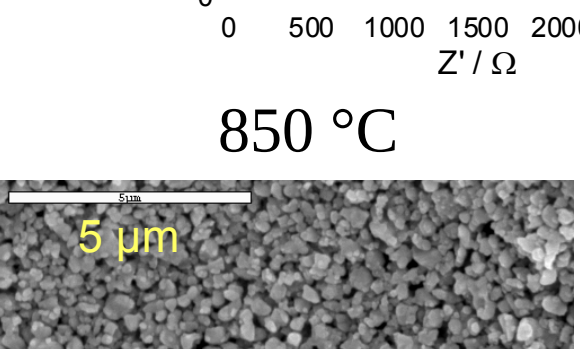

950 °C

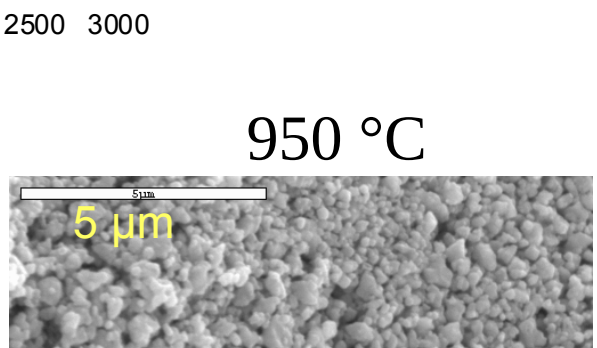

1100 °C

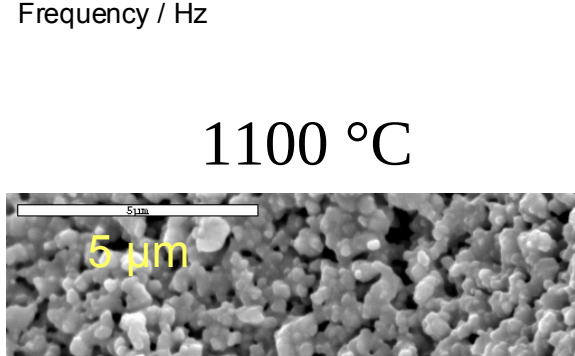

Highest temperature coarsens microstructure - multiple changes to impedance

Powder supplied by NexTech

VERIFY ELECTROCHEMICAL PERFORMANCE ASPECTS OF MODEL

Microstructure/Impedance - LSF Sintering Temperature Effect

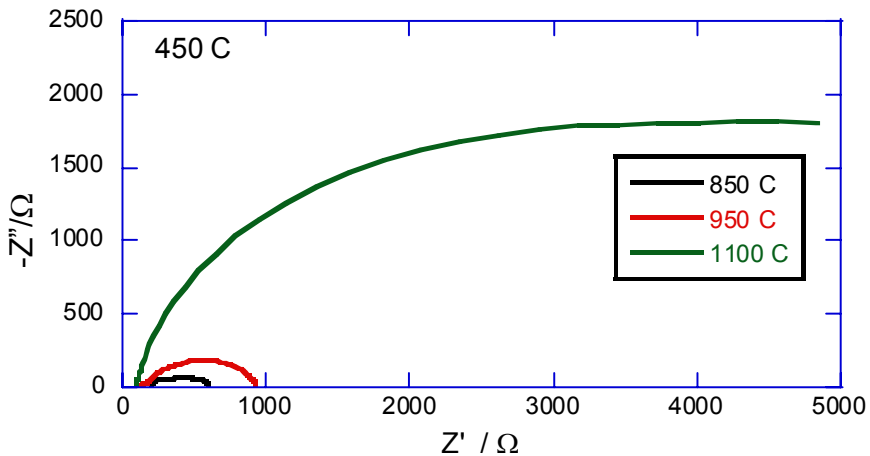

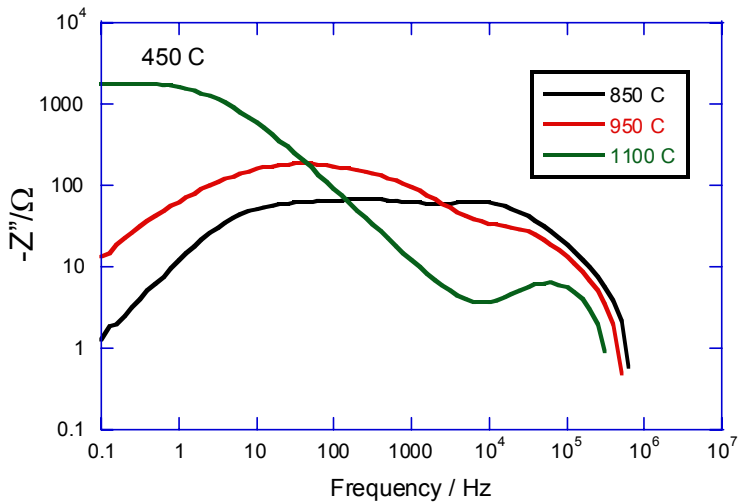

850 °C

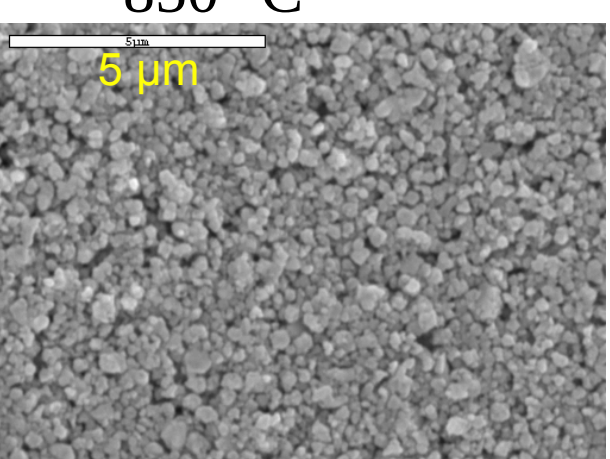

950 °C

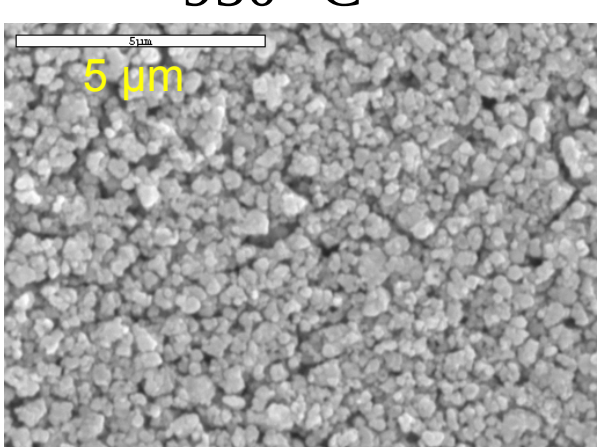

1100 °C

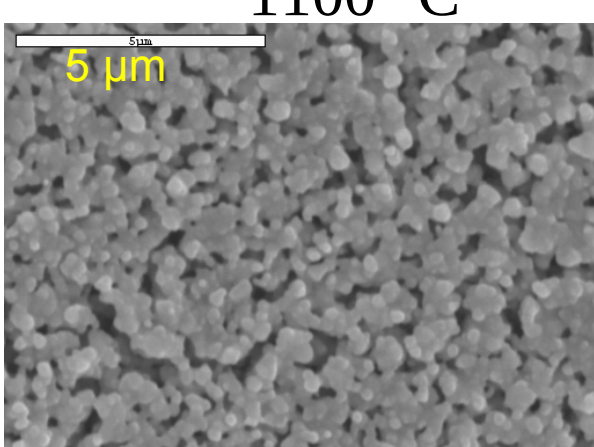

Highest temperature coarsens microstructure - multiple changes to impedance

Powder supplied by NexTech

VERIFY ELECTROCHEMICAL PERFORMANCE ASPECTS OF MODEL

Microstructure/Impedance - LSF Pore-Former Effect

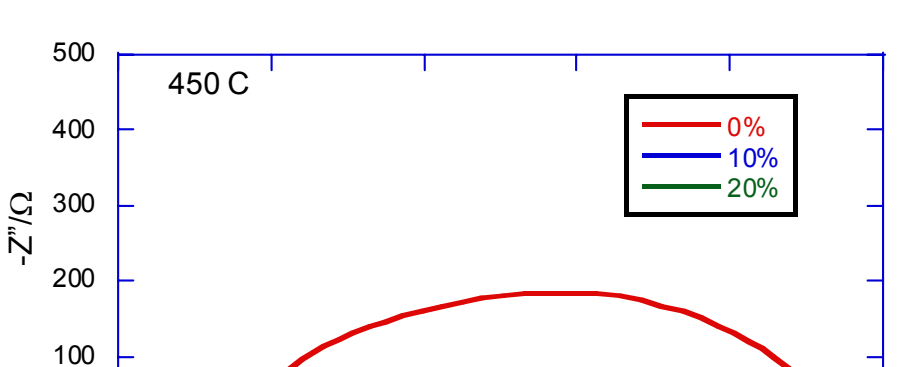

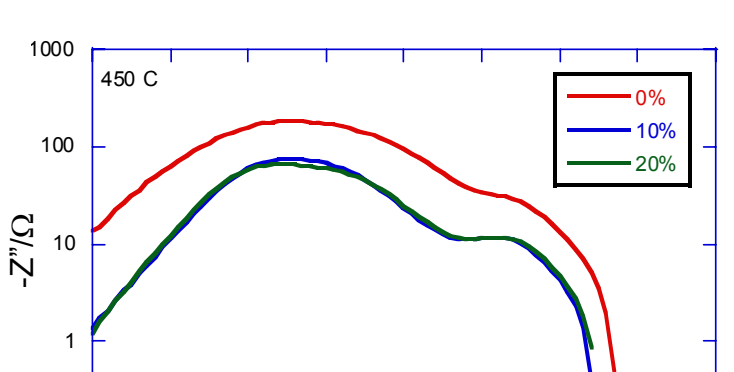

0% added

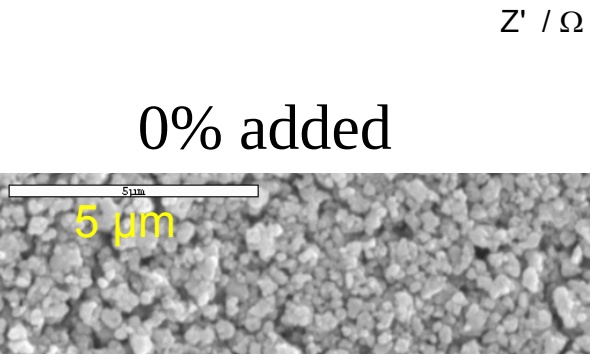

10% added

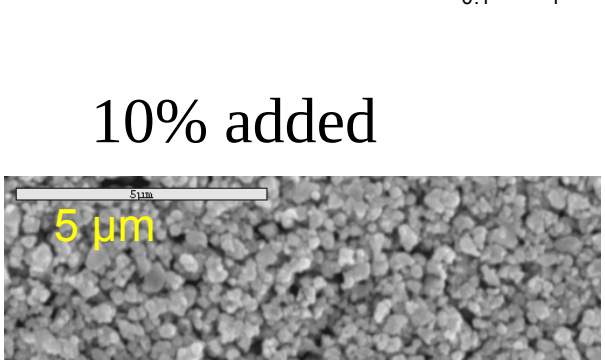

20% added

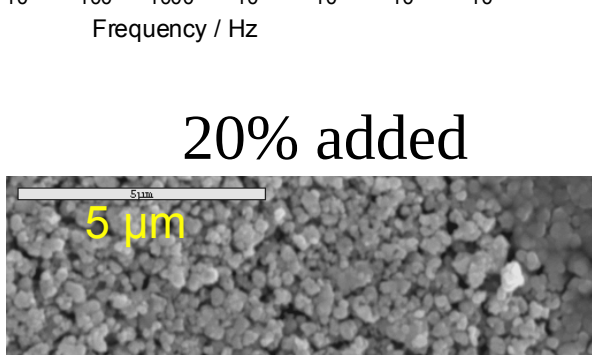

10% and 20% have lowest impedance

Powder supplied by NexTech

VERIFY ELECTROCHEMICAL PERFORMANCE ASPECTS OF MODEL

Microstructure/Impedance - LSCF Pore-Former Effect

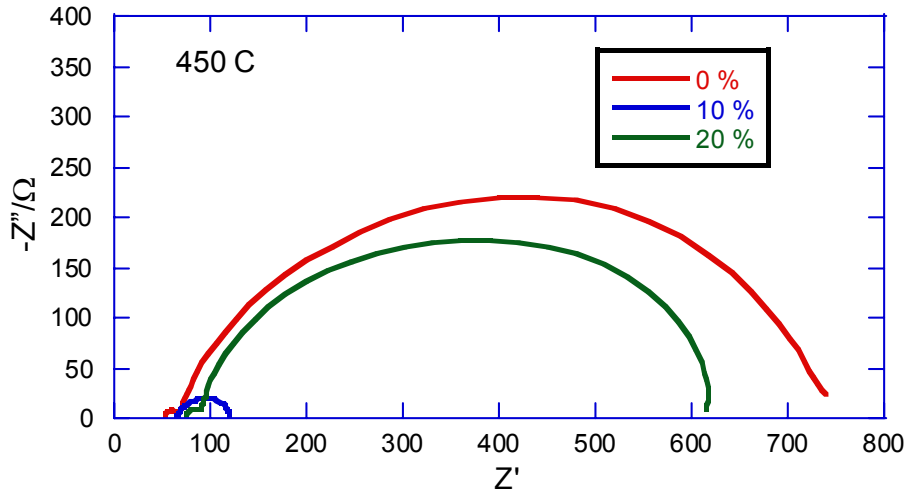

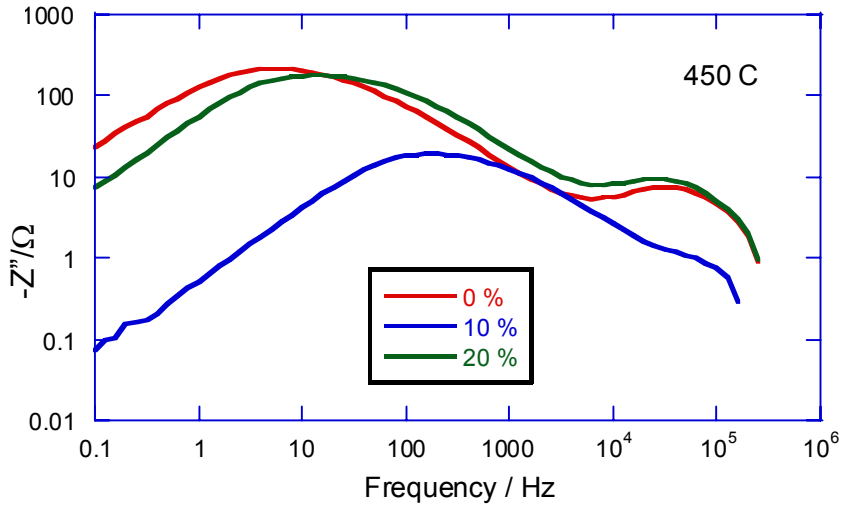

0% added

10% added

20% added

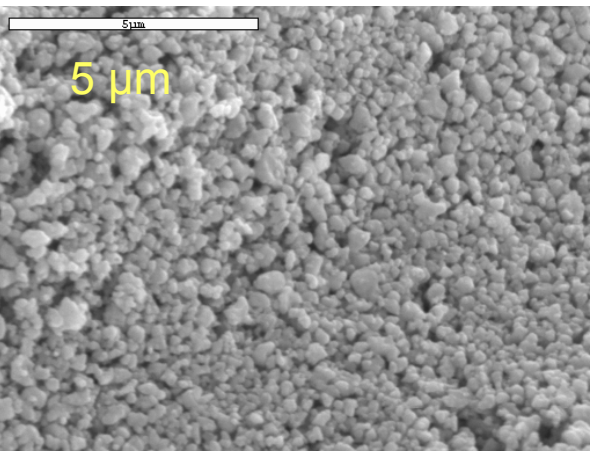

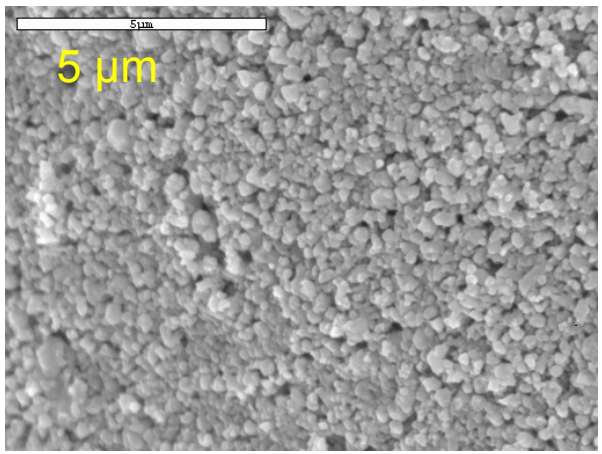

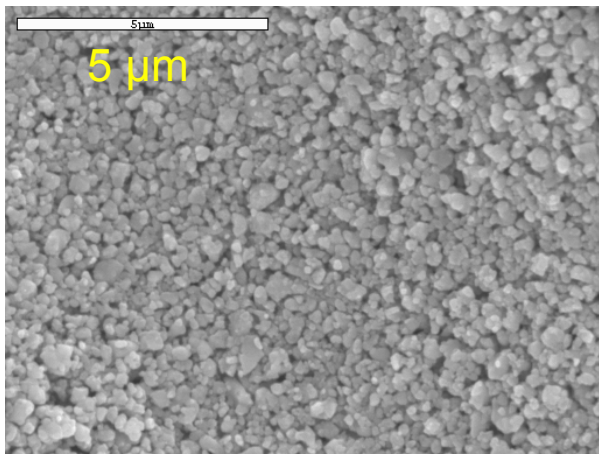

10% optimum - Why?

Powder supplied by NexTech

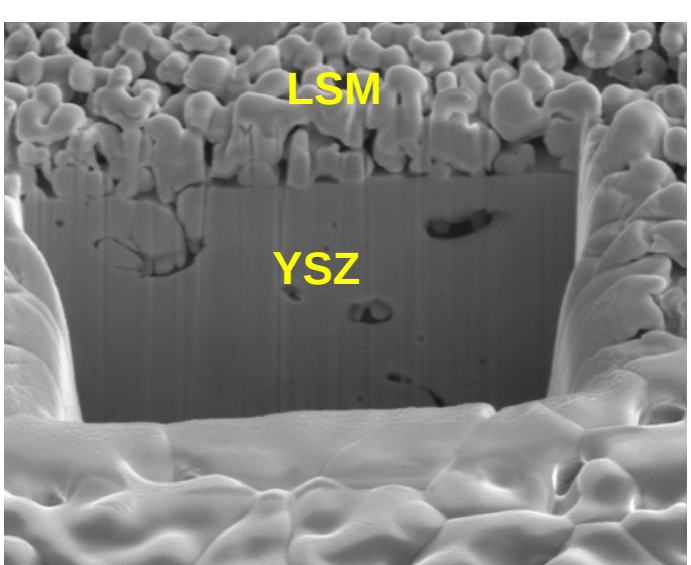

Focused Ion Beam

- Enables 3-D analysis of electrode microstructure
  - Particle-size, pore-size, & distribution
  - Triple-phase boundary density
  - Tortuosity

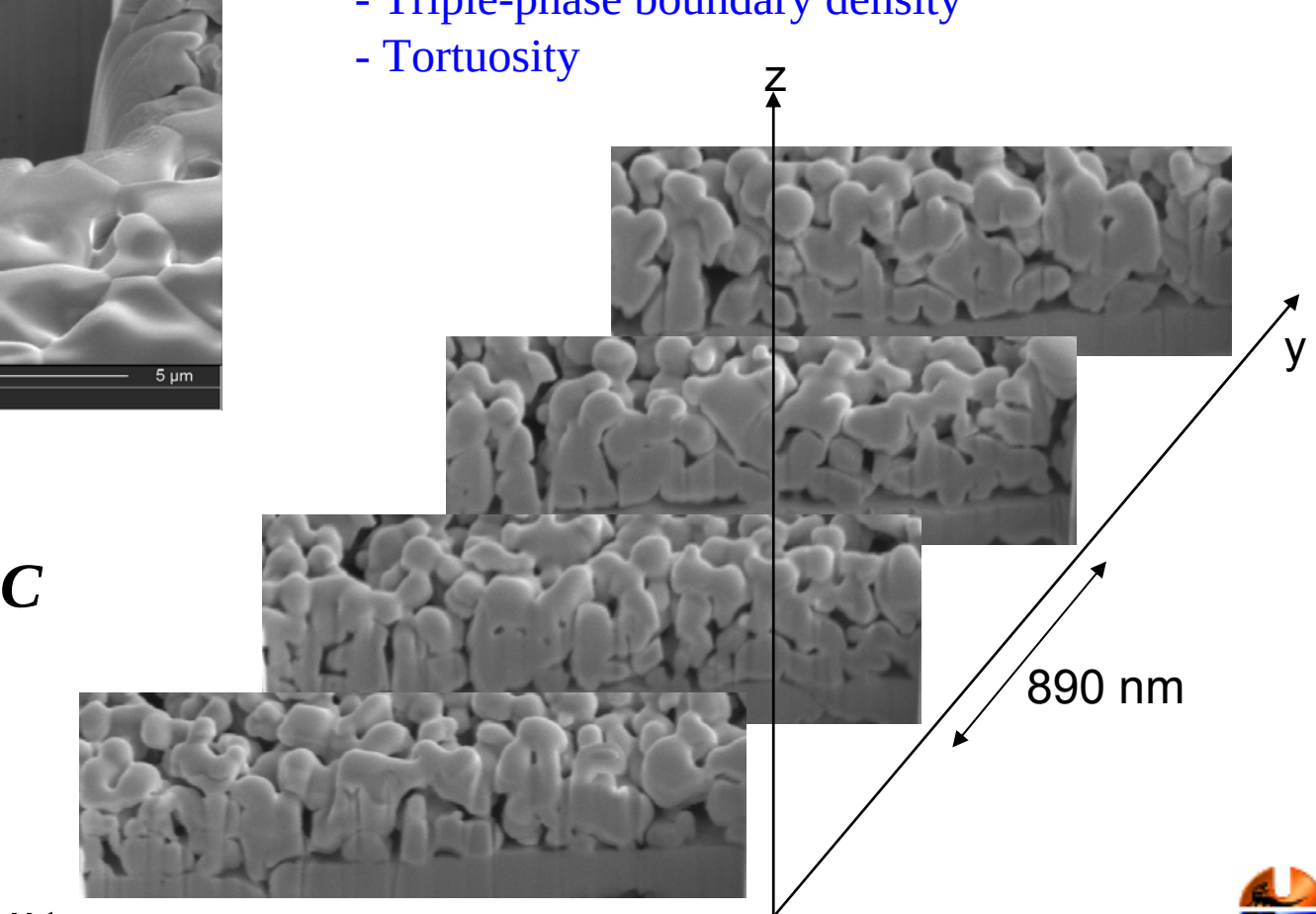

UF-DOE HiTEC

VERIFY CHEMICAL STABILITY ASPECTS OF MODEL
LSM/YSZ Interface

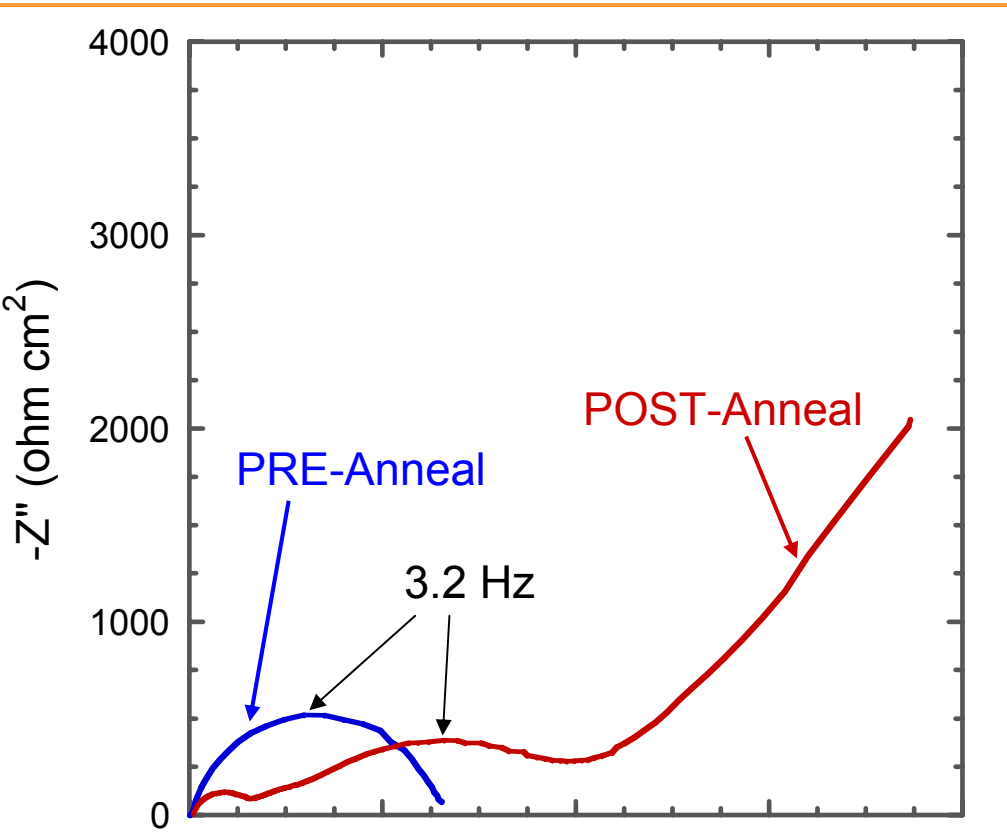

- Annealed at 1400 °C for 48 hours
- Presence of 3.2 Hz resonant frequency in pre- and post-anneal samples indicate that one transport phenomena remains the same
- Additional post-anneal features due to formation of interfacial phase(s)
- Formation of additional phase to be compared with CLEM predictions of interfacial P_{O2}
- Time dependence of growth of additional phase to be compared with transient CLEM

Samples supplied by NexTech

VERIFY CHEMICAL STABILITY ASPECTS OF MODEL
LSM/YSZ Interface

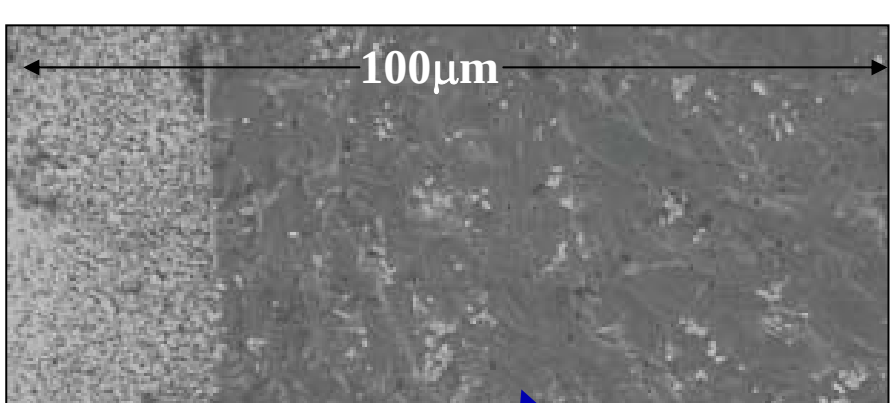

- LSM/YSZ interface **before** and **after** 1400ºC 48 hr anneal.

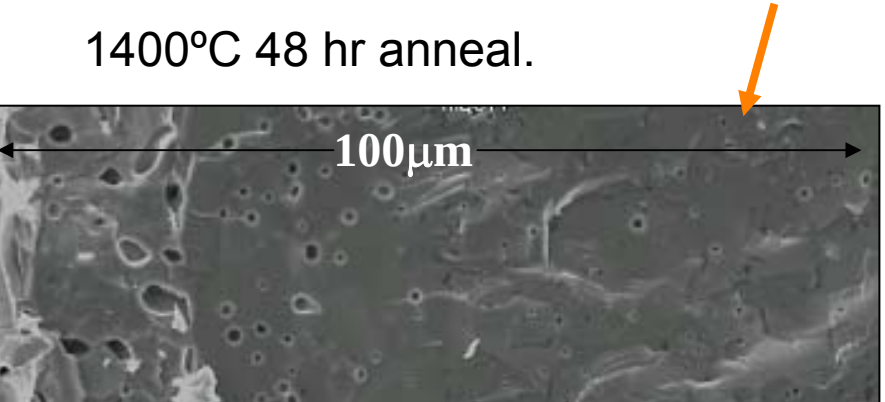

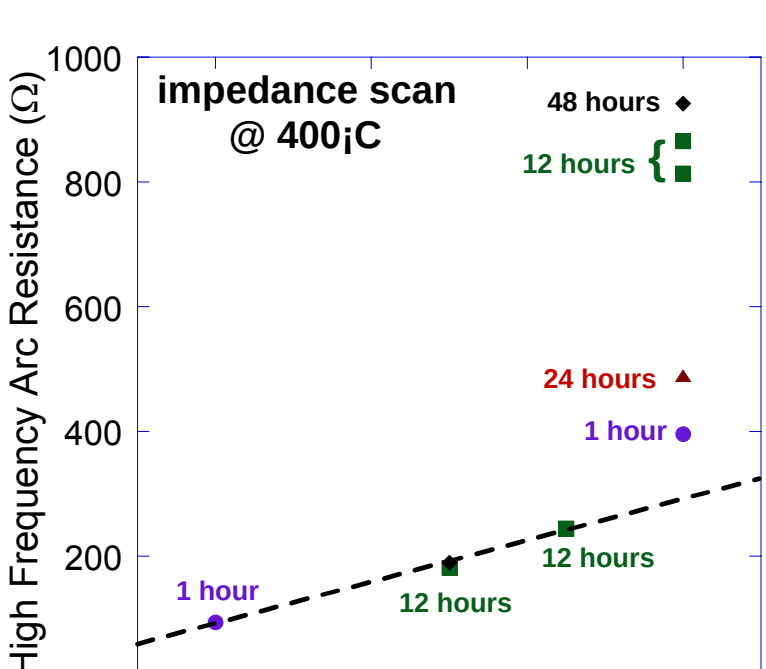

VERIFY CHEMICAL STABILITY ASPECTS OF MODEL
LSM/YSZ Interface

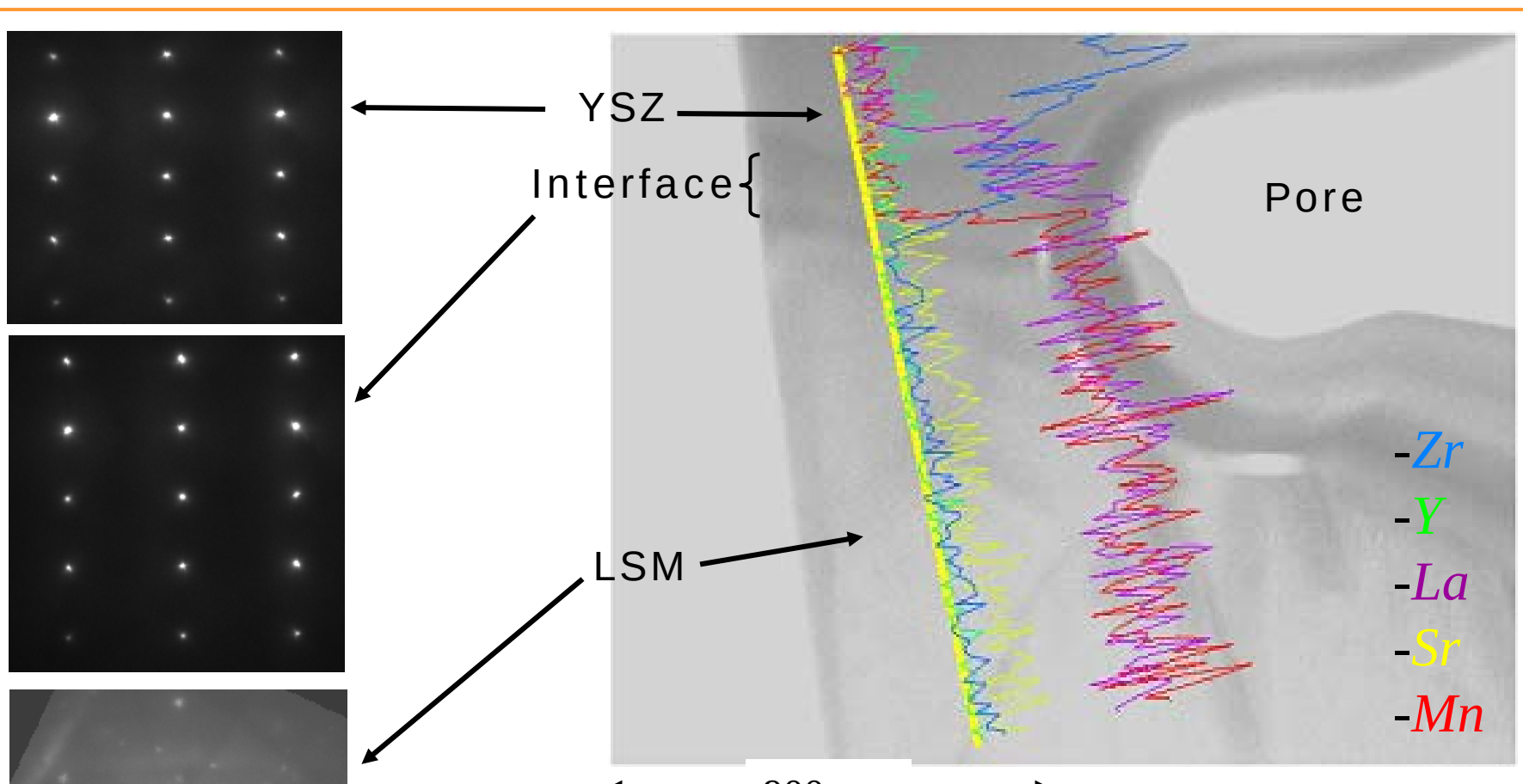

Formation of $La_2Zr_2O_7$ at LSM/YSZ interface

EXTENSION OF MODEL TO THERMO-MECHANICAL PROPERTIES

- Develop theoretical relationships between Vacancy concentration (c_v) and mechanical properties

- Validate experimentally:

  -Vacancy concentration as a function of P_{O_2} (Cahn Microbalance)

  $c_v = f(T, P_{O_2})$ -> K(T)

  -Thermal expansion as a function of P_{O_2} (THETA Dilatometer)

  $\Delta L \sim \Delta c_v = f(T, P_{O_2})$

  -Bulk Elastic Moduli and Fracture Toughness (Triboindenter)

  Y and $K_{IC} \sim f(C_v) = f(T, P_{O_2})$

  -Bulk Elastic Moduli (Resonant Ultrasound) - E. Lara-Curzio, ORNL

  $Y \sim f(C_v) = f(T, P_{O_2})$

  -Elastic Moduli and Fracture Toughness of polycrystalline samples (MTS) at high temperature and as a function of P_{O_2}

  Y and $K_{IC} = f(T, P_{O_2}$, microstructure)

EXTENSION OF MODEL TO THERMO-MECHANICAL PROPERTIES
Theory Development

QuickTime™ and a
TIFF (LZW) decompressor
are needed to see this picture.

$$E_{bond} = \frac{A}{r^m} - \frac{B}{r^n}$$

A, B, n and m are constants

Lattice constant, a, has linear relationship with c_v

Therefore, $r \sim a \sim c_v$

M. O. Zacatea, L. Minervinia, D. J. Bradfielda, et.al. *Solid State Ionics* 128(2000) 243.
D-J. Kim, *J. Amer. Ceram. Soc.* 72 (1989) 1415.

EXTENSION OF MODEL TO THERMO-MECHANICAL PROPERTIES
Dilatometer Results

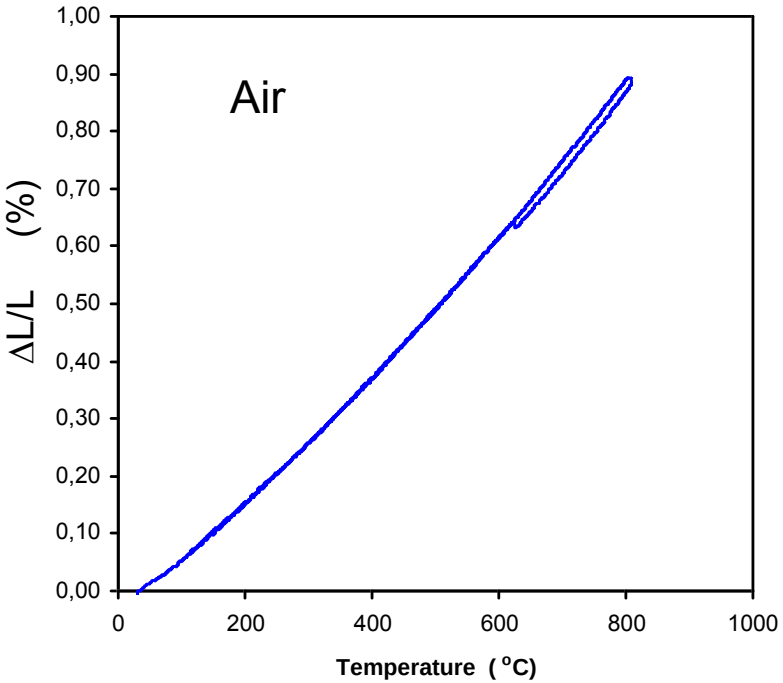

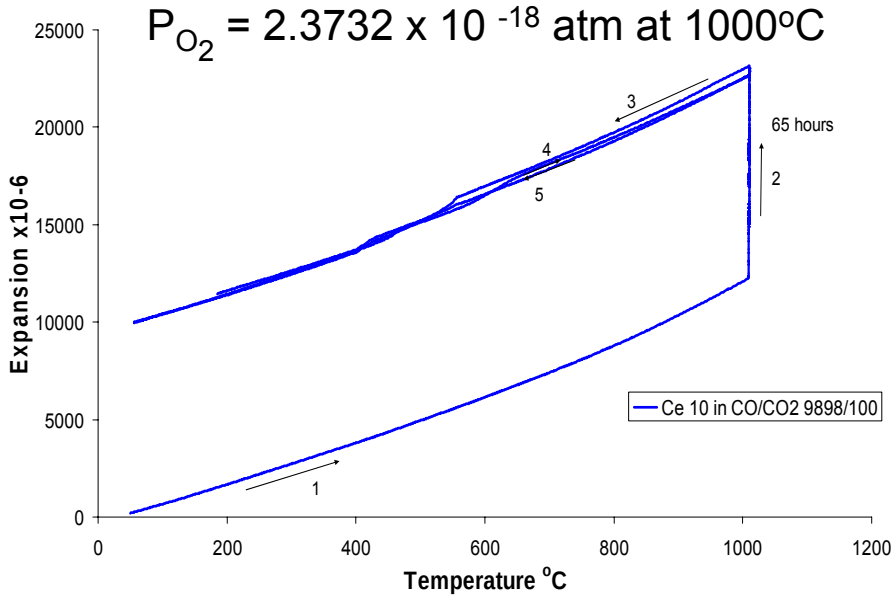

Similar results obtained at ORNL

- Measured with Theta® dilatometer
- Initial length 12.1 mm CeO_2
- CTE / 10^{-6} $^oC^{-1}$

Temp	CTEx 10^{-6}
700°C	12.2 $^oC^{-1}$
750°C	12.7 $^oC^{-1}$
800°C	13.2 $^oC^{-1}$
800°C*	13.05 $^oC^{-1}$

*Sameshima *et al.* J.Cer. Soc. of Japan **110** (2002)

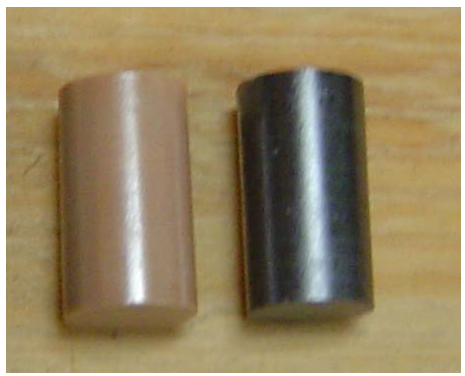

CeO_2- initial & reduced

EXTENSION OF MODEL TO THERMO-MECHANICAL PROPERTIES
Theory Development

$$Y_{bond} = \frac{1}{r_0}\left(\frac{d^2E}{dr^2}\right)_{r=r_0}$$

QuickTime™ and a TIFF (LZW) decompressor are needed to see this picture.

$$E_{bond} = \frac{A}{r^m} - \frac{B}{r^n}$$

A, B, n and m are constants

$$Y \approx Y^*\left(\sqrt[m+3]{Y^*}\theta c_V + 1\right)^{-(m+3)}$$

$Y \sim a^{-(m+3)}$ and $K_{IC} \sim Y^{1/2}a^{-3/2}$

Lattice constant, a, has linear relationship with c_v

Therefore, $r \sim a \sim c_V$

$$K_{IC} \approx K_{IC}^*\left(\sqrt[m+6]{\left(K_{IC}^*\right)^2}\beta c_V + 1\right)^{-\frac{m+6}{2}}$$

M. O. Zacatea, L. Minervinia, D. J. Bradfielda, et.al. *Solid State Ionics* 128(2000) 243.
D-J. Kim, *J. Amer. Ceram. Soc.* 72 (1989) 1415.

EXTENSION OF MODEL TO THERMO-MECHANICAL PROPERTIES
Spatial Variation of Modulus (Y) & Fracture Toughness (K_{IC})

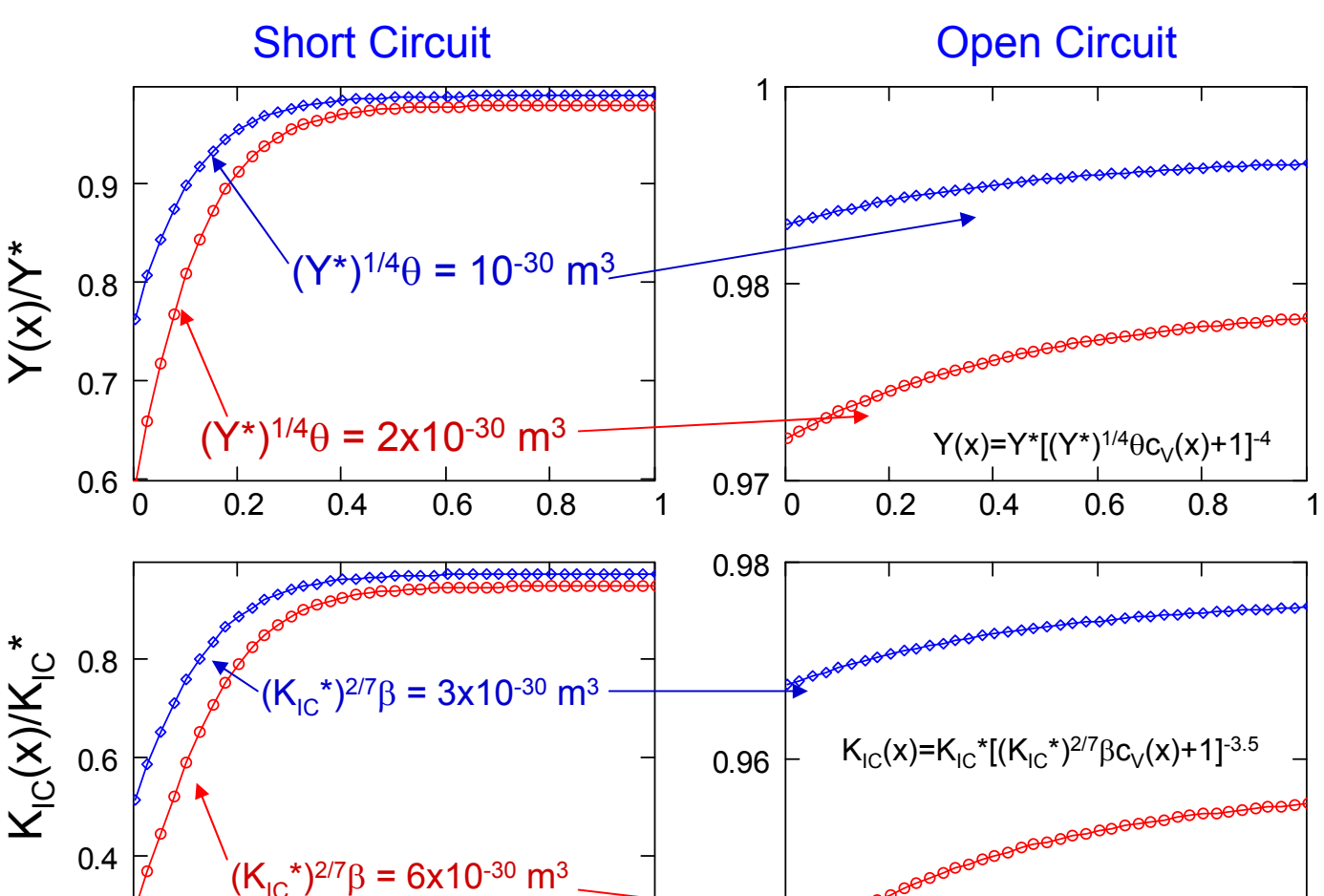

Indicates mechanical failure at anode under high current, consistent with LBL results*

*S. Visco, SECA, Albany, NY, Oct. 2003

EXTENSION OF MODEL TO THERMO-MECHANICAL PROPERTIES
Bulk Elastic Moduli (Resonant Ultrasound) - E. Lara-Curzio, ORNL

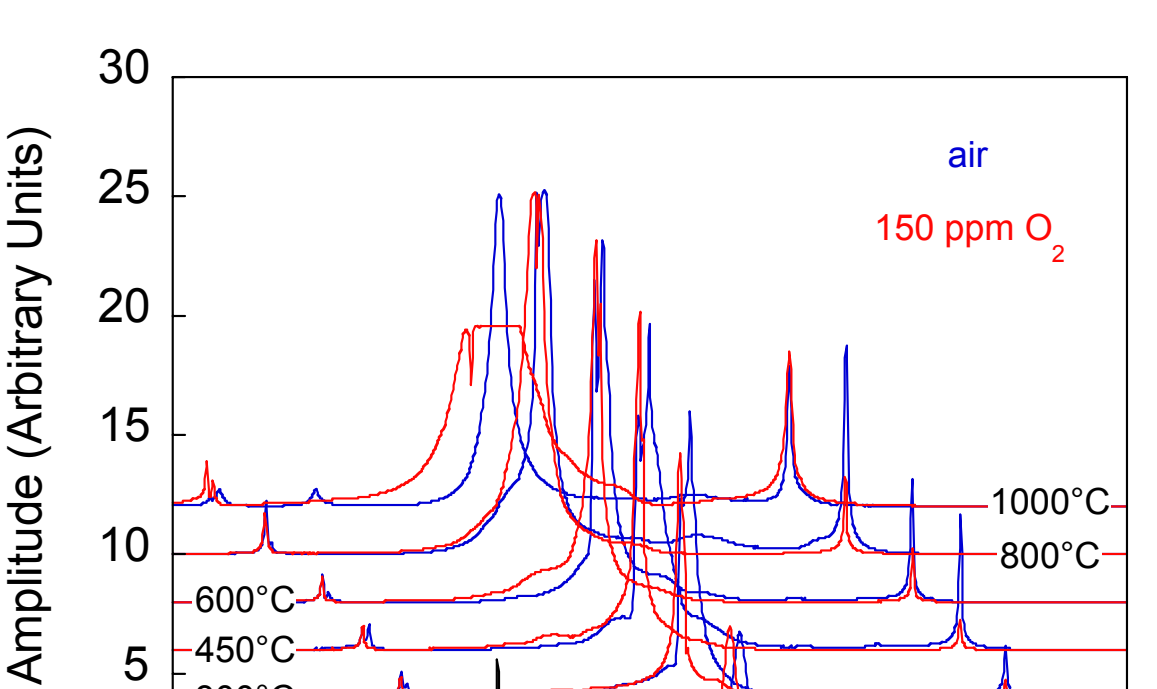

Broadening of peaks and shift to lower frequency indicate weaker bonds and lower modulus under low P_{O2}, consistent with model predictions.

$$Y \sim f(C_v) = f(T, P_{O_2})$$

Evolution of resonant ultrasound spectrum as a function of temperature for tests carried out in air (blue peaks) or in an environment with 150 ppm of O_2 (red peaks).

More than 40 peaks were used to estimate the magnitude of the elastic properties.

EXTENSION OF MODEL TO THERMO-MECHANICAL PROPERTIES
Experimental Validation

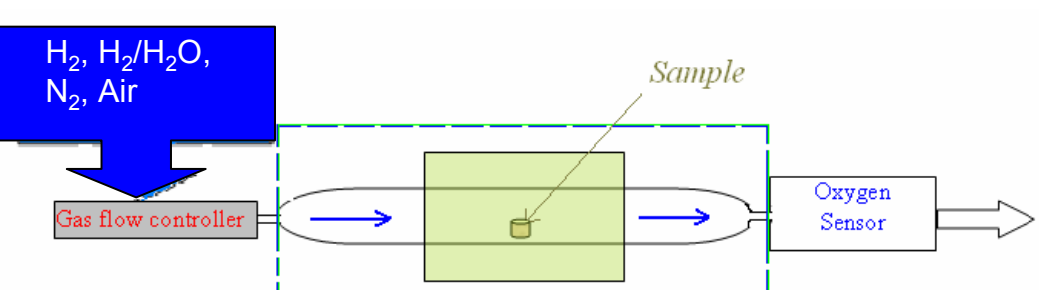

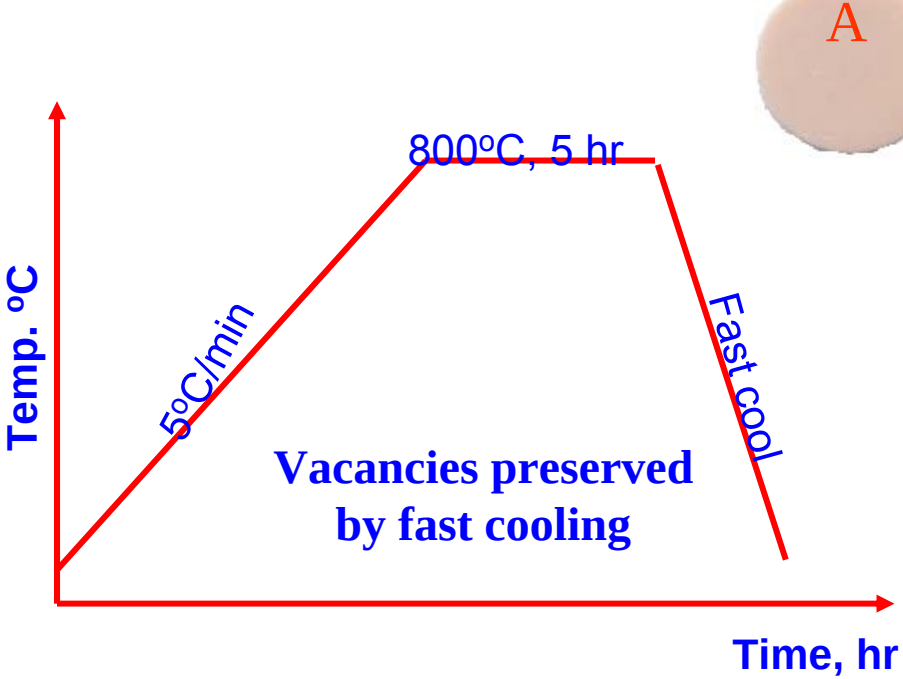

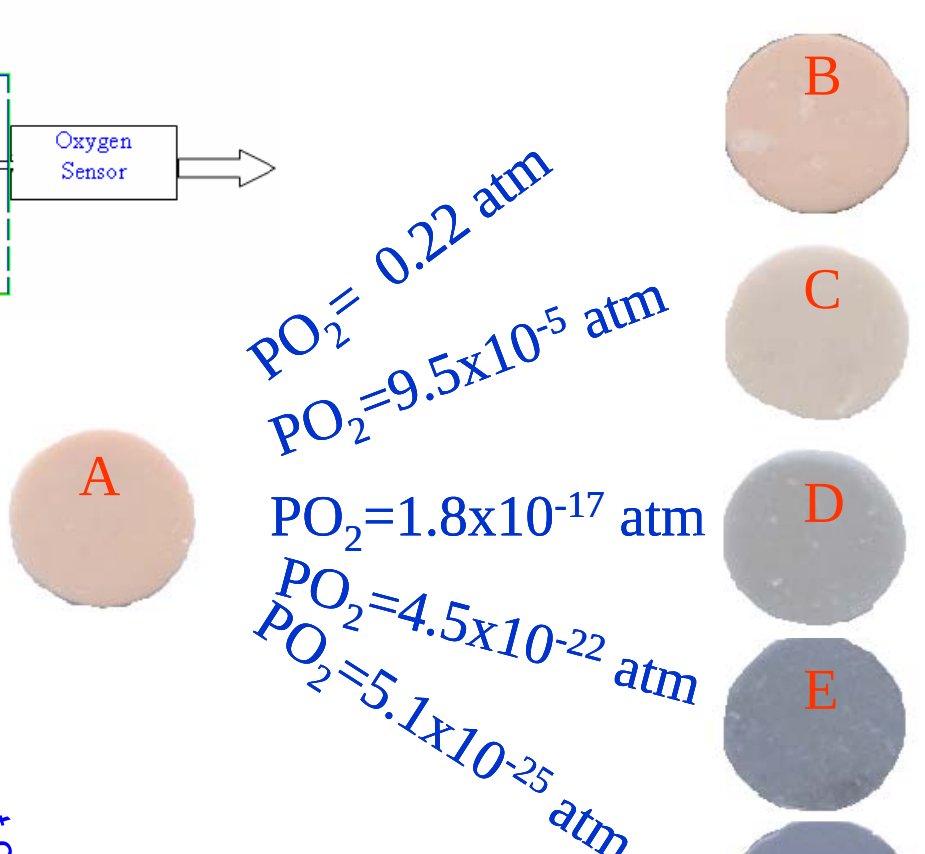

EXTENSION OF MODEL TO THERMO-MECHANICAL PROPERTIES
Experimental Validation - Nanoindentation

Hysitron TriboIndenter

(Major Analytical Instrumentation Center)

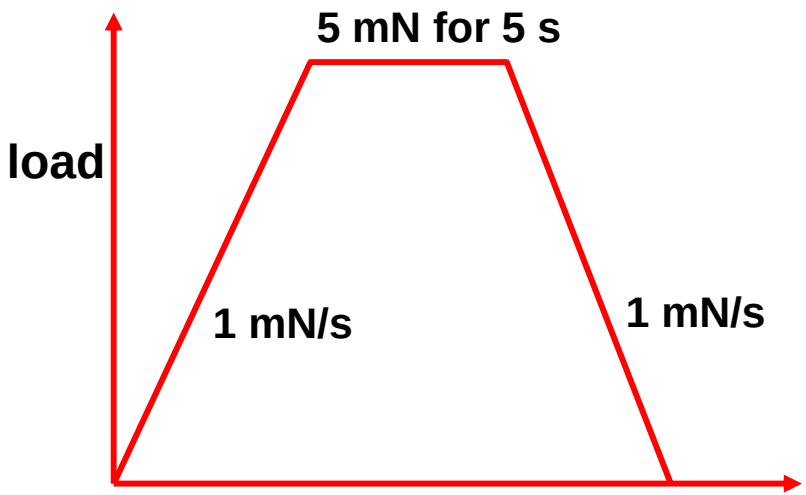

Load Function

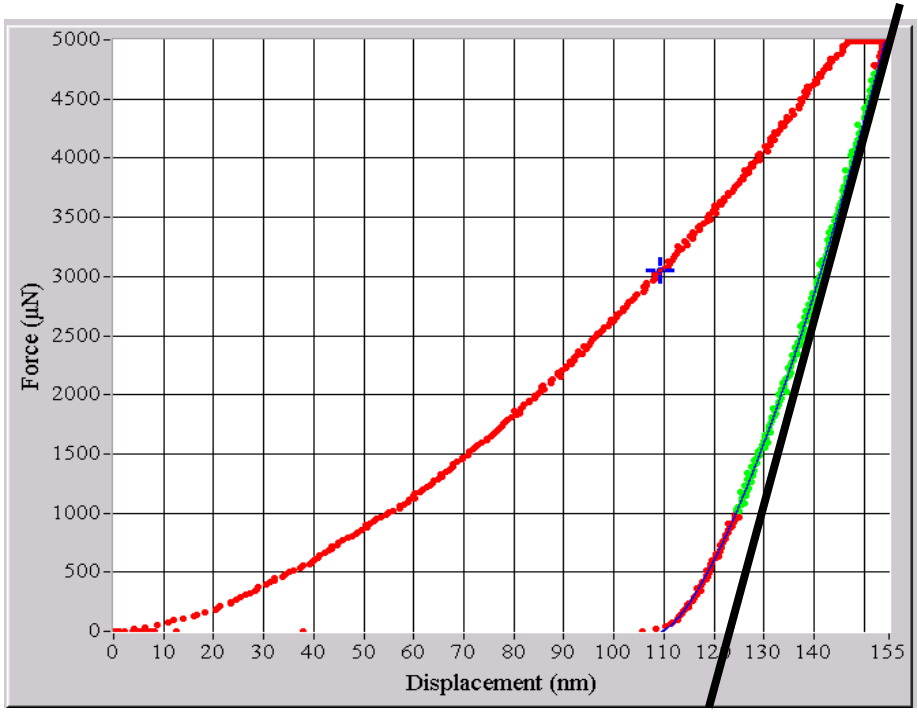

Reduced Modulus (Y_r) is calculated from the slope of the unloading segment

$$\frac{1}{Y_r} = \frac{(1-\upsilon^2_{indentor})}{Y_{indenter}} + \frac{(1-\upsilon^2_{ceria})}{Y_{ceria}}$$

ν is the poisson ratio

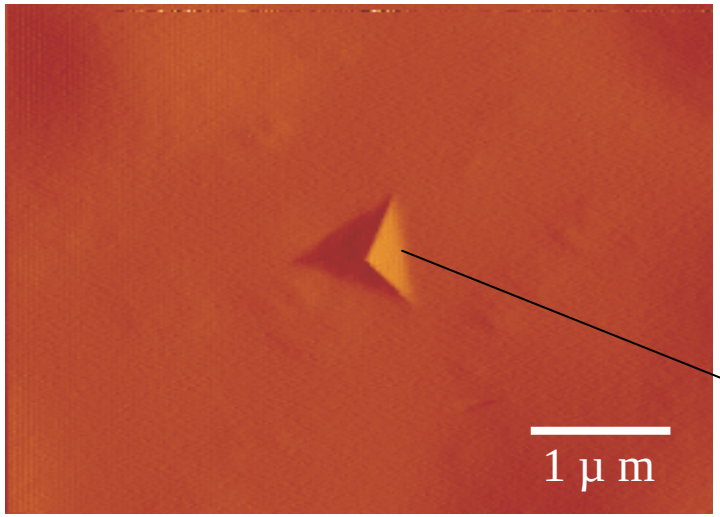

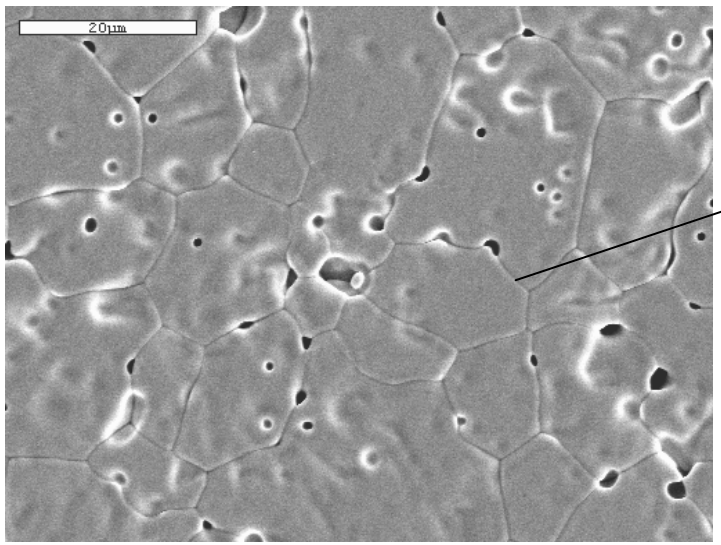

SEM image of surface after thermal etch.
Average grain size ~12 µm.

Nanoindents

Size: **~0.6 µm**

Depth: **~125 nm**

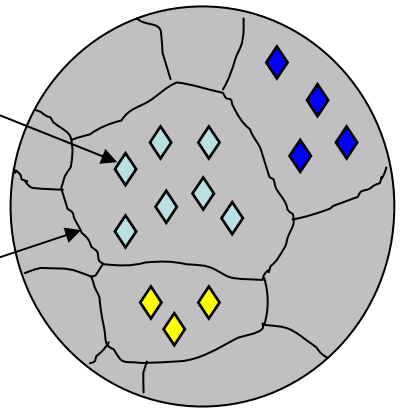

•Effect of crystallographic orientation on elastic modulus and hardness evaluated statistically by applying many indents on grains of known orientation.

•In-plane anisotropy can be measured by changing the indent orientation.

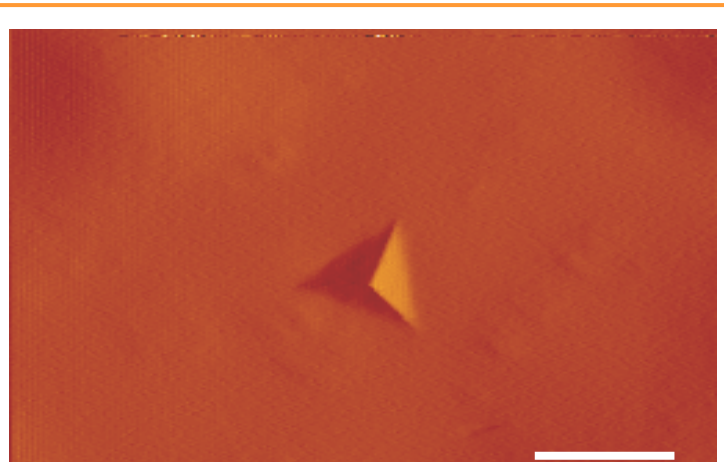

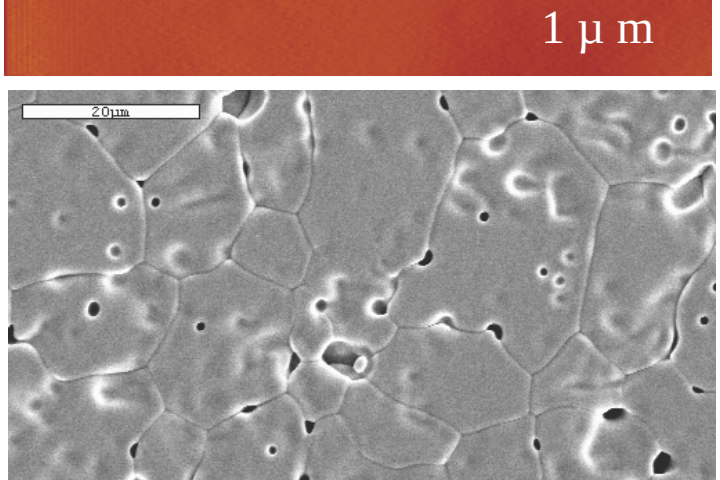

SEM image of surface after thermal etch.
Average grain size ~12 µm.

Nanoindents

Size: **~0.6 µm**

Depth: **~125 nm**

- **100 indents were applied on the sample, which covered 100 µm X 100 µm (~25 different grains)**

Modulus: 218.35±11.12 GPa

Hardness: 9.00±0.73 Gpa

- **The small variations imply that ceria is elastically isotropic.**

Effect of Oxygen Vacancy Population on Elastic Modulus of

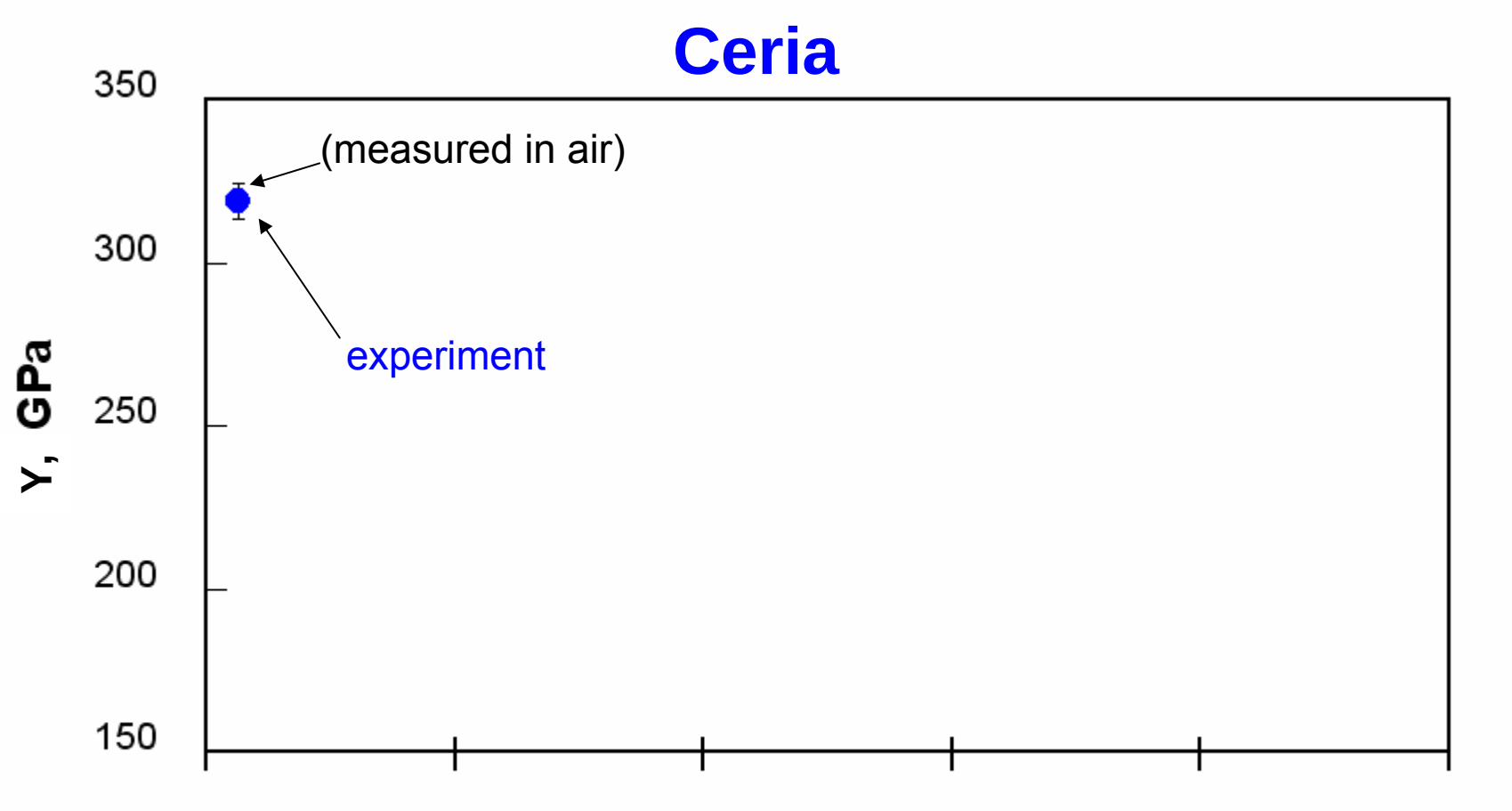

Effect of Oxygen Vacancy Population on Elastic Modulus of

Ceria

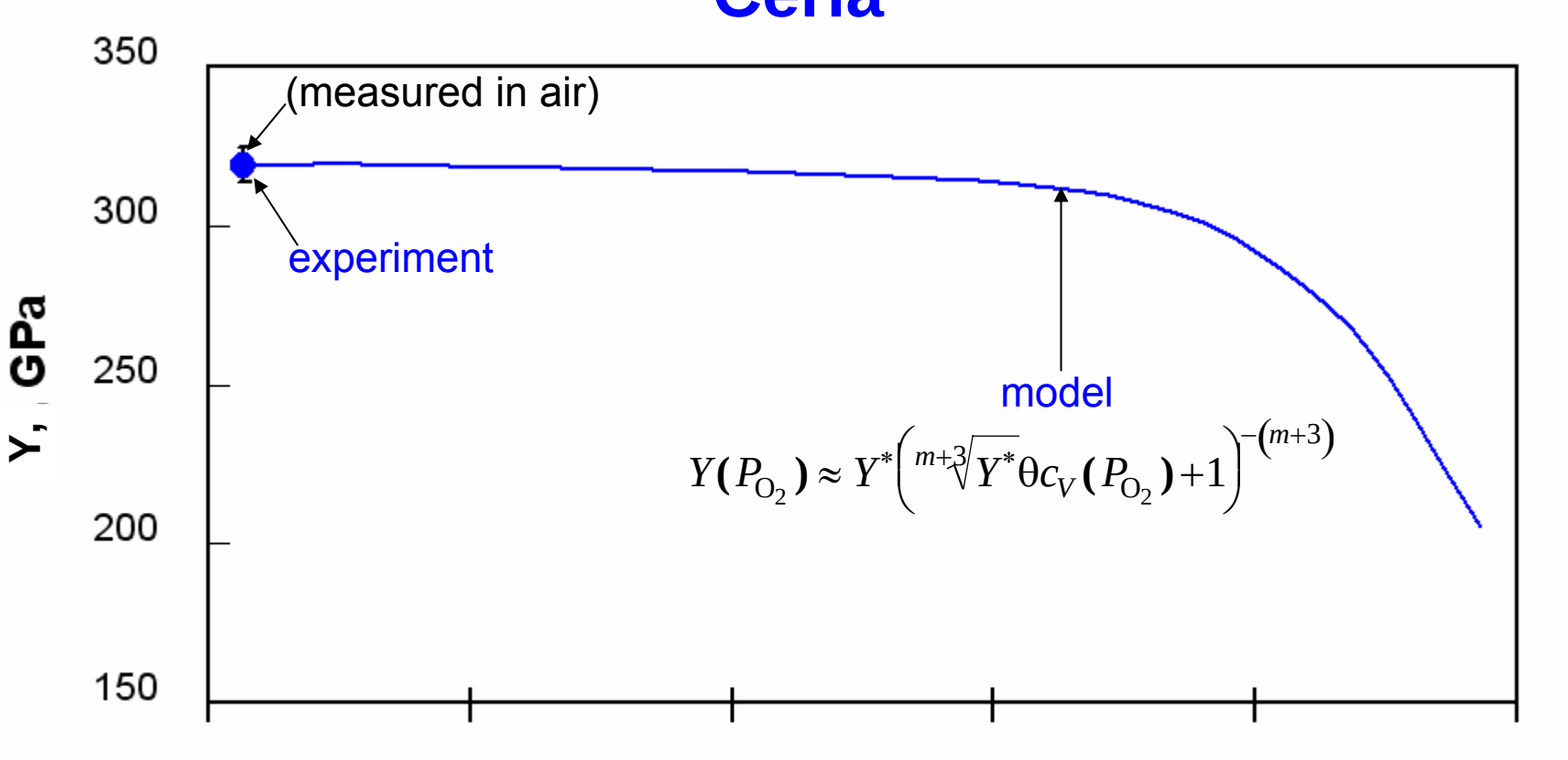

Effect of Oxygen Vacancy Population on Elastic Modulus of

Ceria

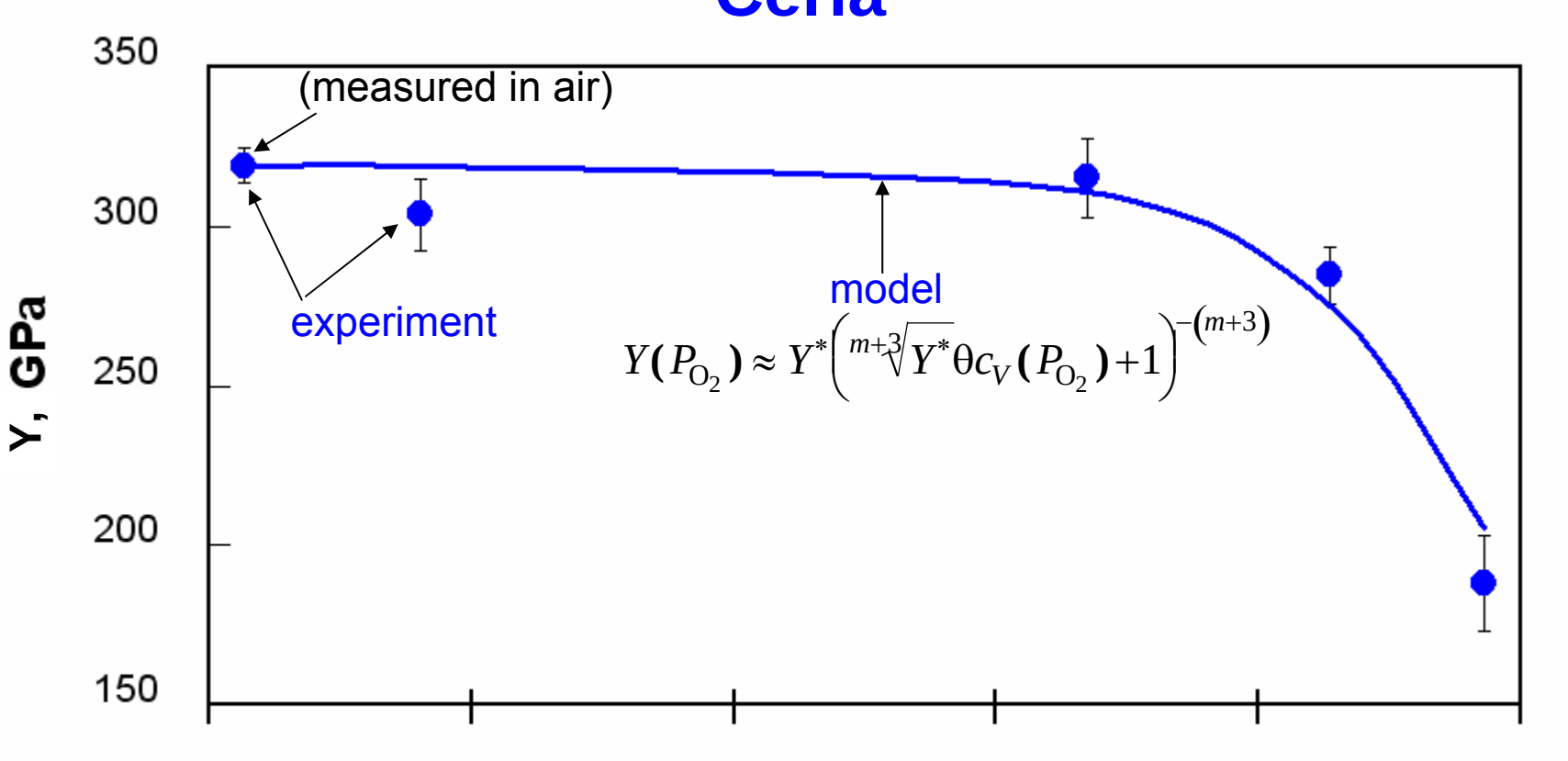

Effect of Oxygen Vacancy Population on Elastic Modulus of

Gadolinia-Doped Ceria (GDC)

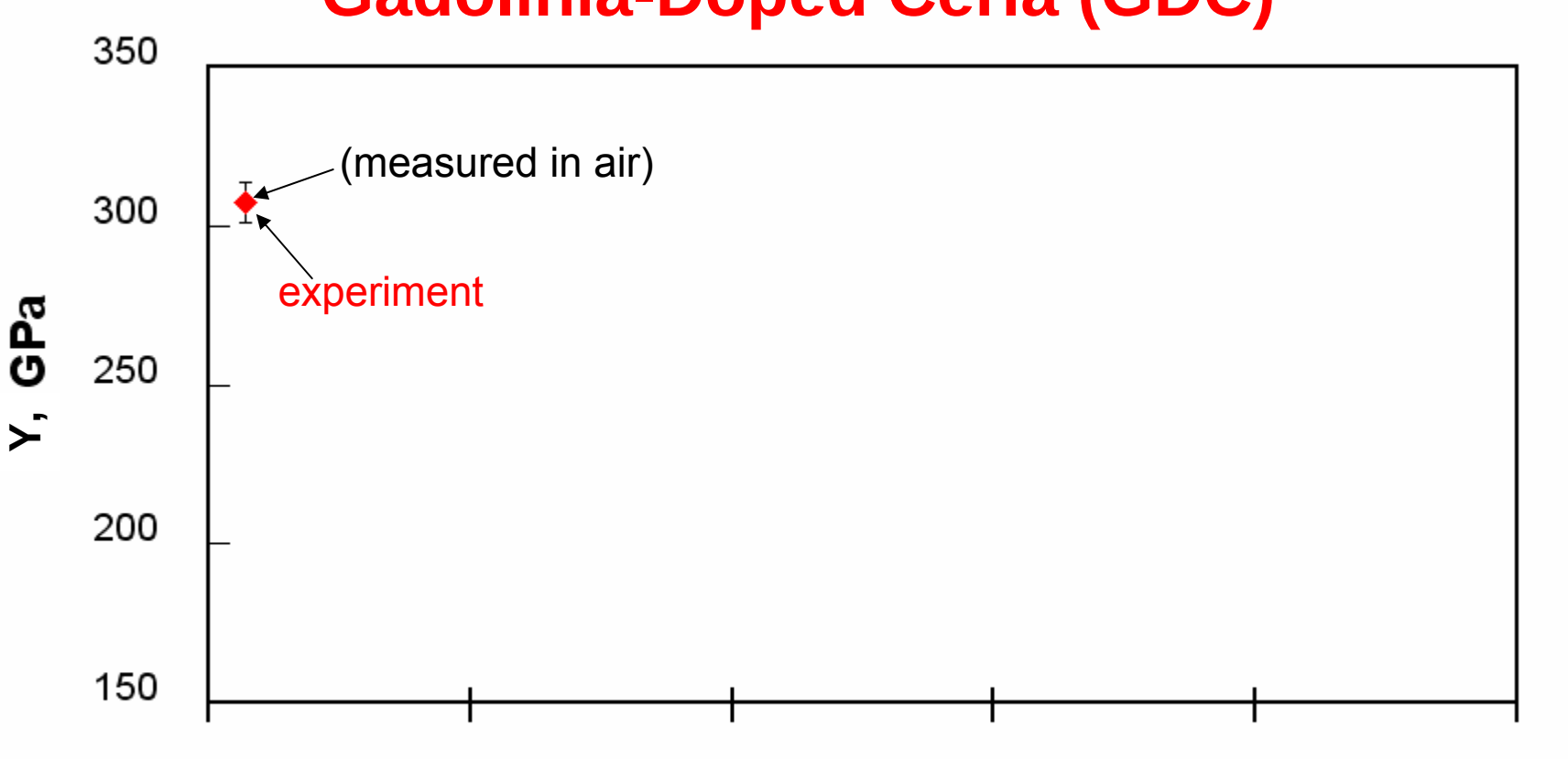

Effect of Oxygen Vacancy Population on Elastic Modulus of

Gadolinia-Doped Ceria (GDC)

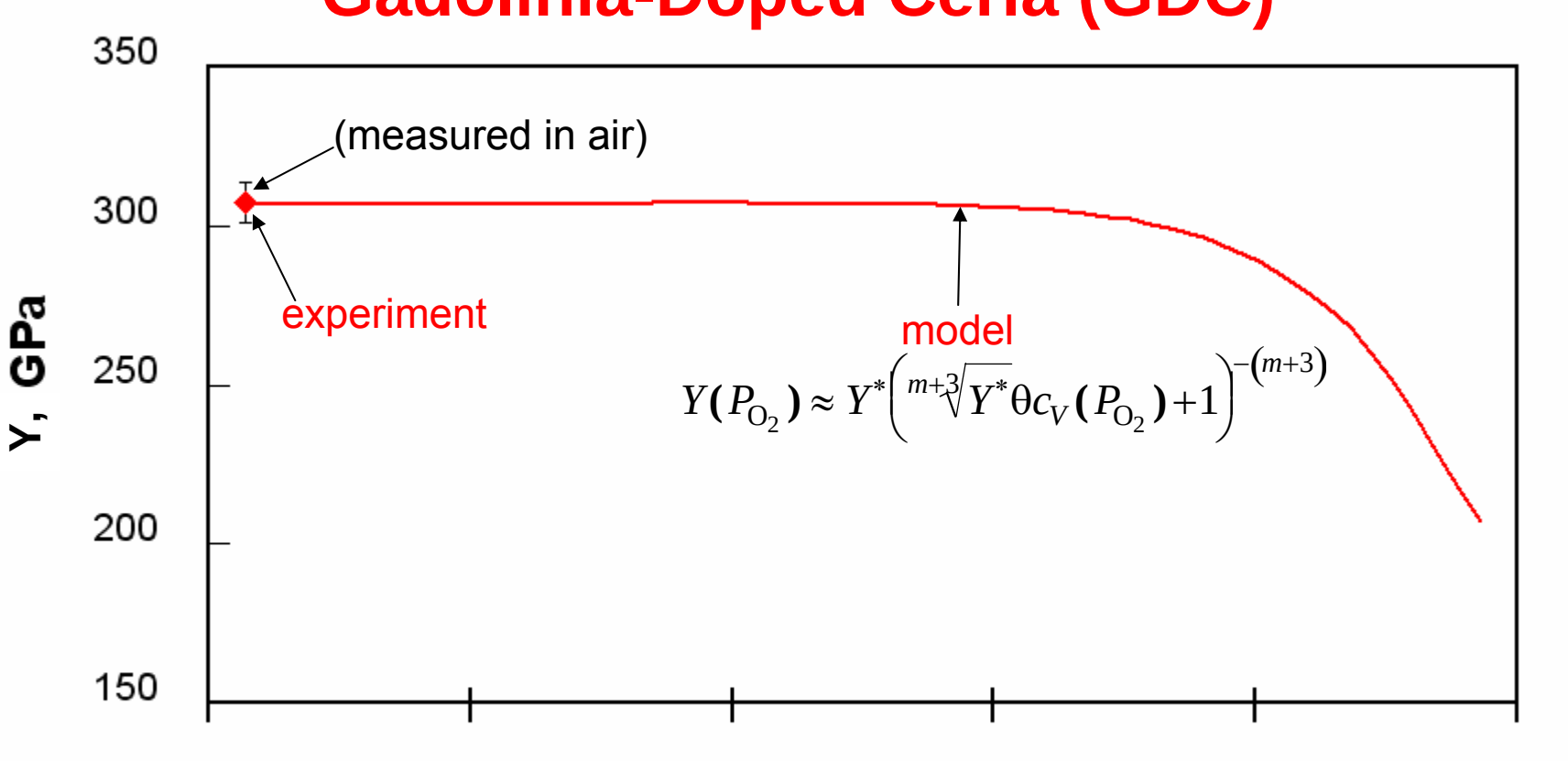

Effect of Oxygen Vacancy Population on Elastic Modulus of

Gadolinia-Doped Ceria (GDC)

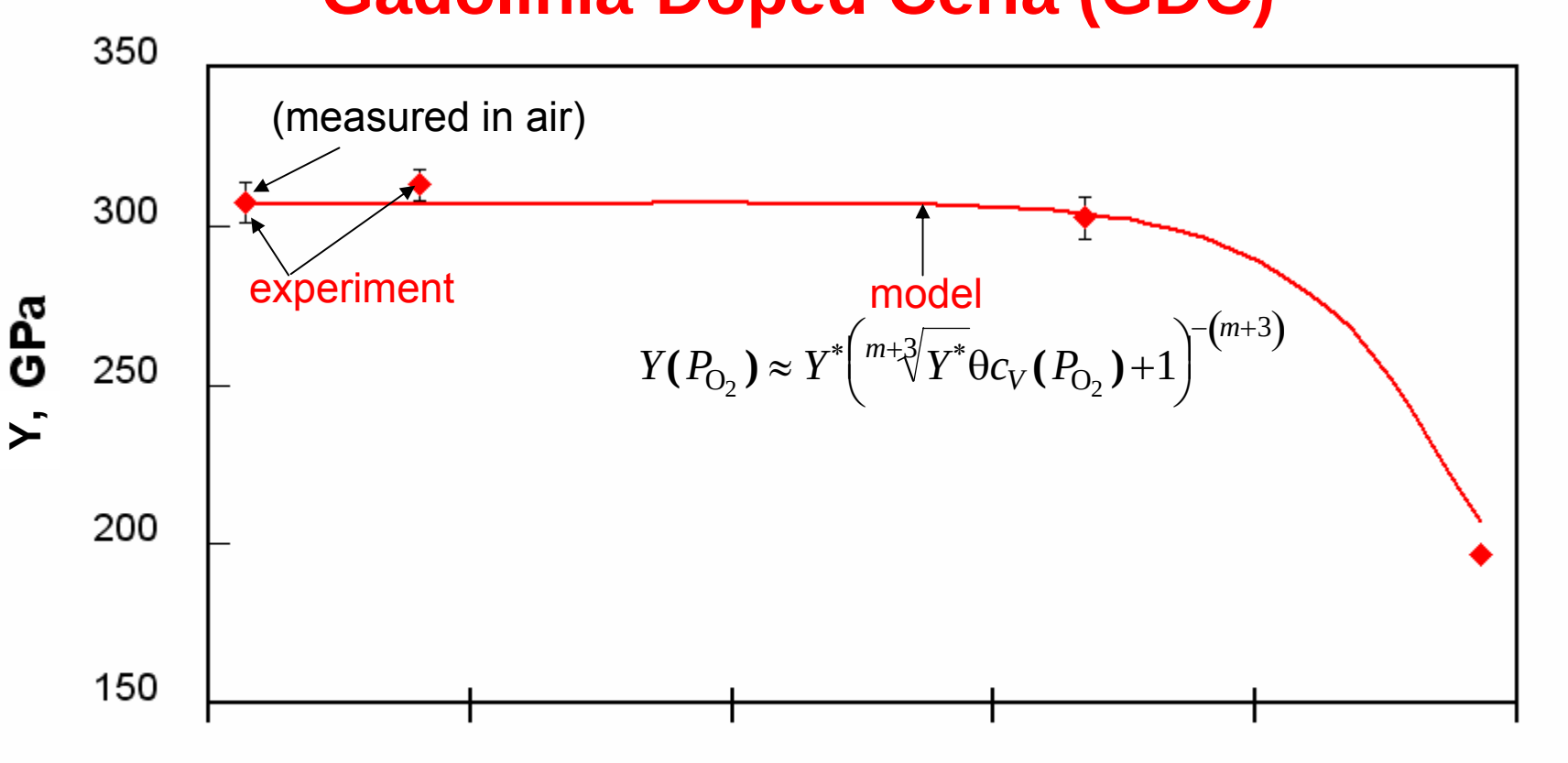

Effect of Oxygen Vacancy Population on Elastic Modulus of

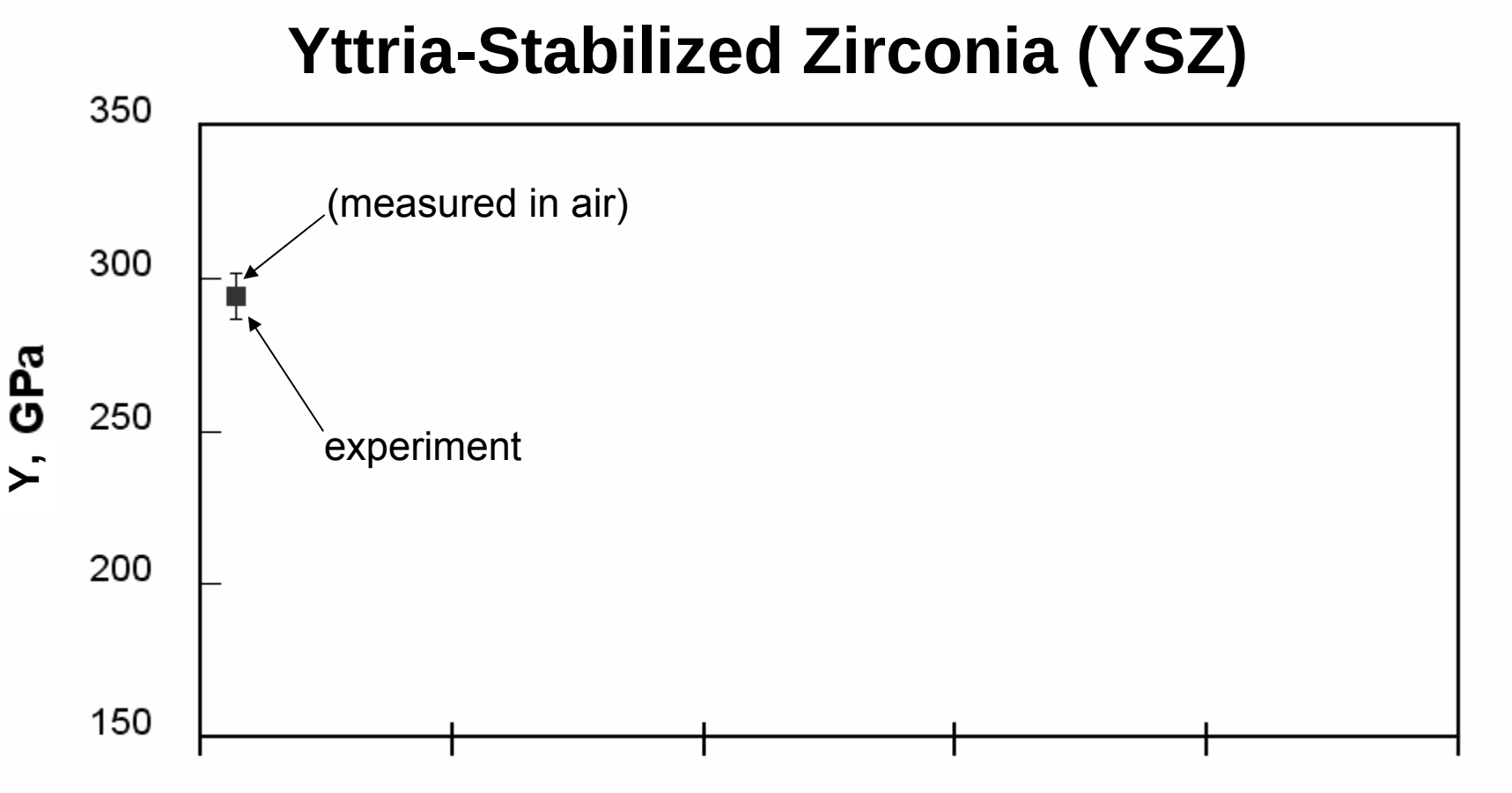

Effect of Oxygen Vacancy Population on Elastic Modulus of

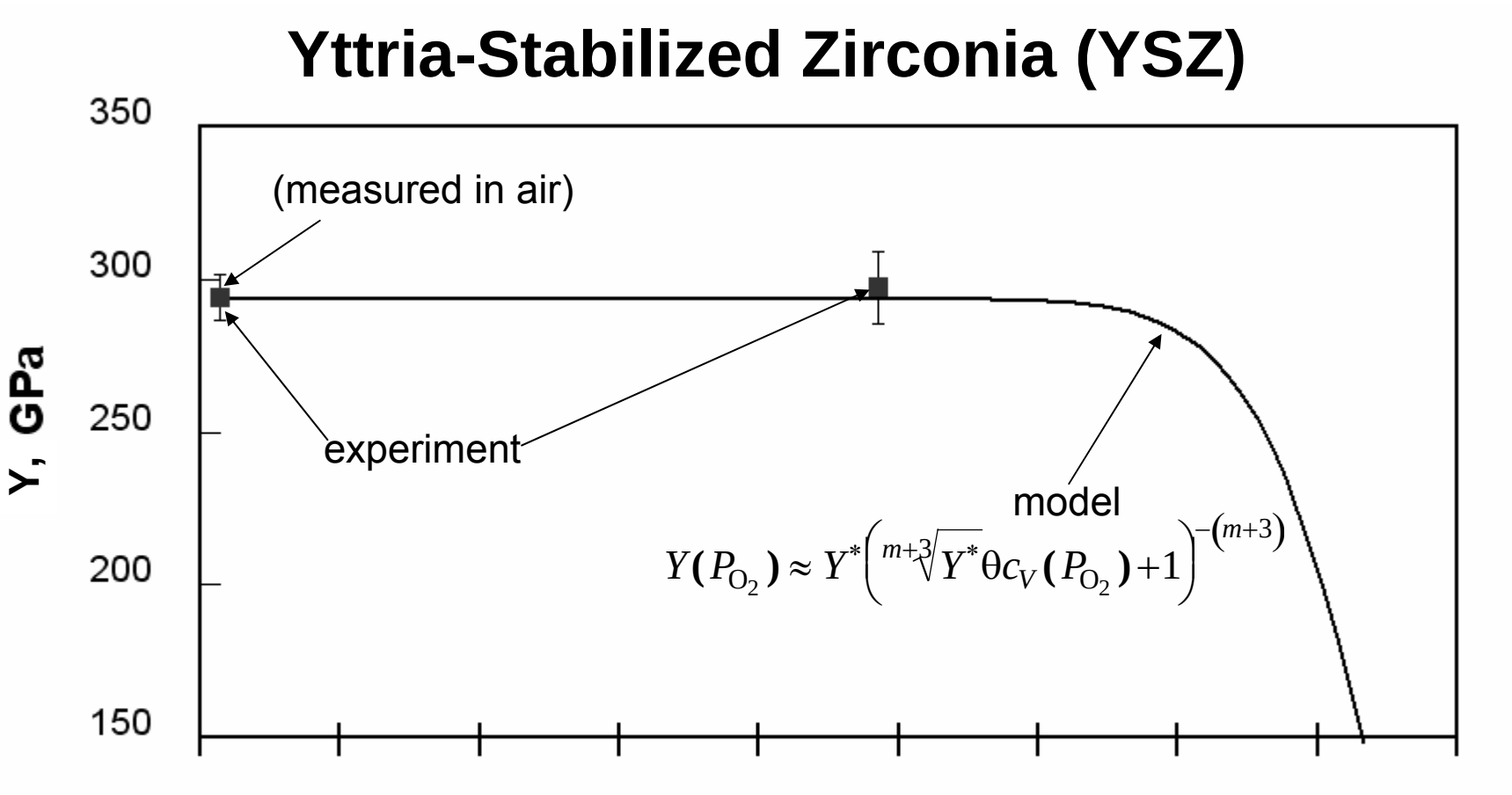

Effect of Oxygen Vacancy Population on Elastic Modulus of

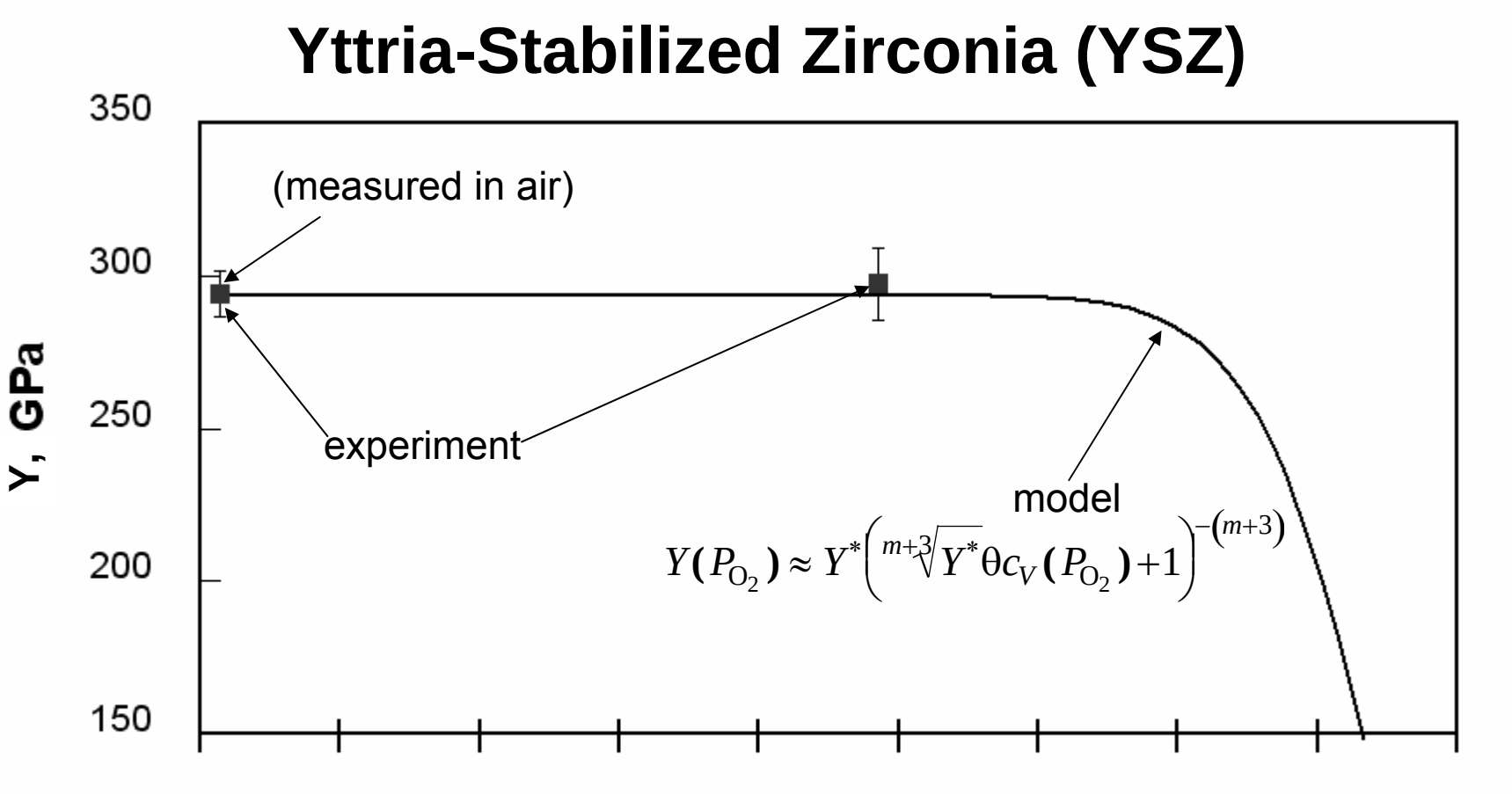

Higher temperature and higher current will shift decrease in modulus to higher P_{O2}

Effect of Oxygen Vacancy Population on Elastic Modulus of

Ceria, GDC,YSZ

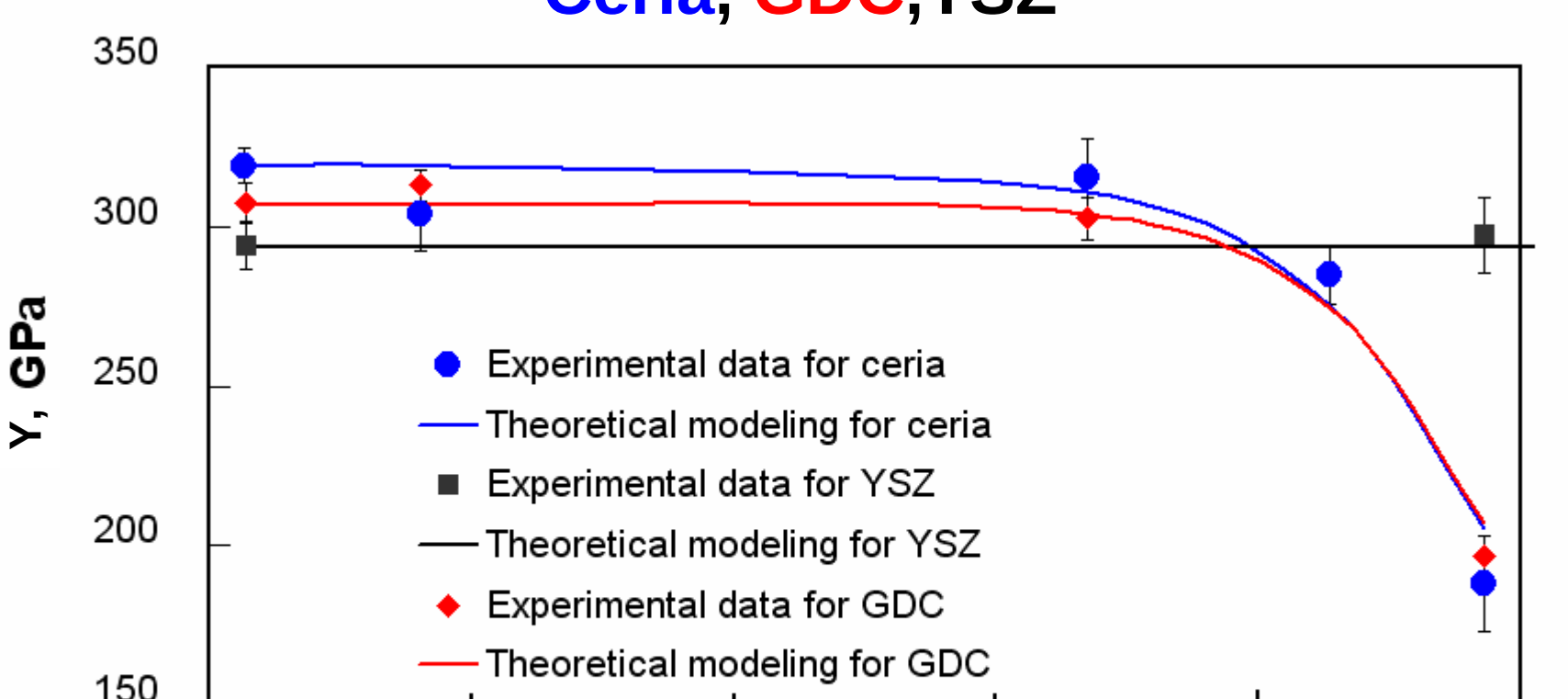

$$Y(P_{O_2}) \approx Y^*\left(\sqrt[m+3]{Y^*}\theta c_V(P_{O_2})+1\right)^{-(m+3)}$$

$\theta Y^{*1/(m+1)} = 10^{-28.9} m^3$ & m = 1 (for ionically bonded ceramics)

CONTINUUM LEVEL ELECTROCHEMICAL MODEL
Defect Equilibria

FLUORITE

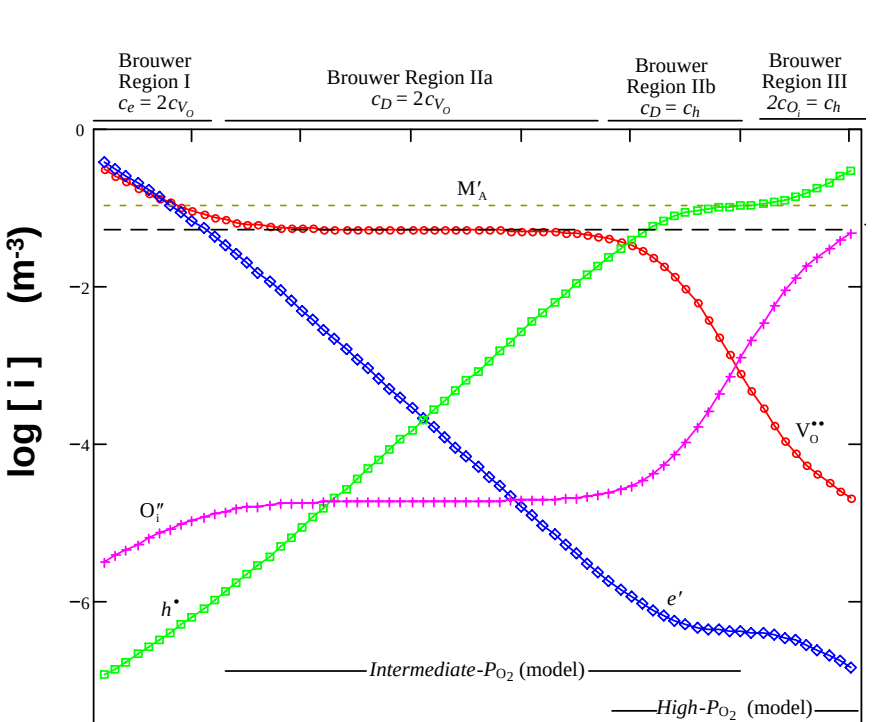

PEROVSKITE

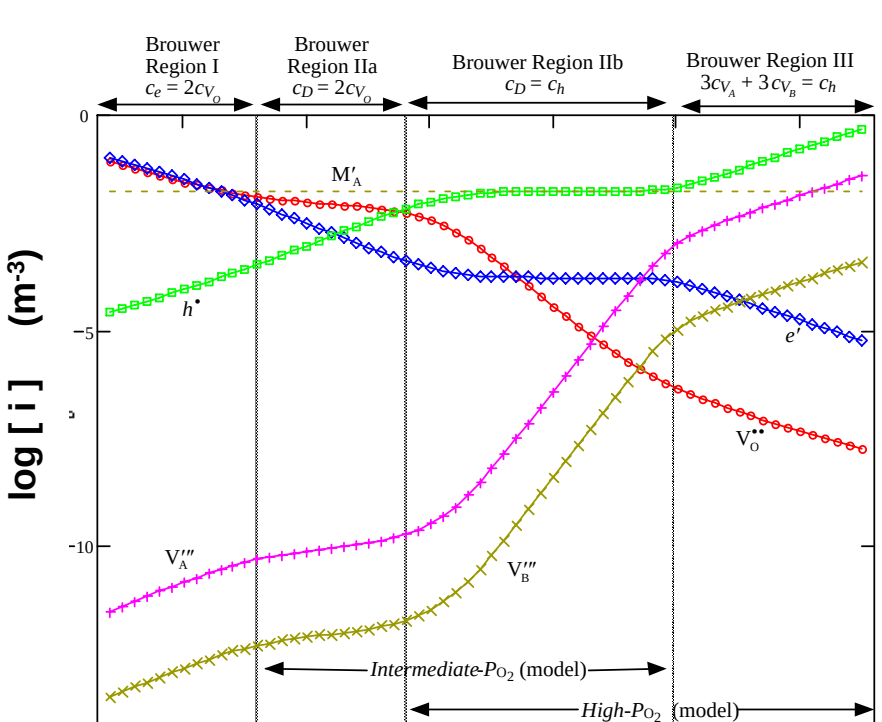

Similar approach should be applied to perovskites

Vo°° concentration changes over typical operating conditions

EXTENSION OF MODEL TO THERMO-MECHANICAL PROPERTIES
Experimental Validation - Microstructural Effects

Four-point bending test using smooth and notched samples

- MTS Testing system equipped with vacuum furnace and controlled atmosphere allows mechanical testing to be conducted up to 1600 °C under a variety of P_{O_2}
- Four-point bend tests used to measure Y and K_{IC} of polycrystalline samples
- Statistical analysis employed to ensure repeatable and reliable results.

For polycrystalline samples

Y and $K_{IC} \sim f(C_v) = f(T, P_{O_2})$

What is affect of microstructure?

CONCLUSIONS

- Developed relationships based on defect thermodynamics and fundamental transport equations that predict defect concentration:
  - Environment (function of P_{O2} and temperature)
  - Potential (function of voltage)
  - Spatial (function of distance through material)
  - Temporal (function of time) and Transient behavior
- Extended model to multilayer structures
  - Electrochemical performance
  - Interaction between materials
    - Phase instability ->performance degradation
- Extended model to include effect of electrode microstructure on electrochemical performance
- Extended model to predict mechanical properties as a function of P_{O2} and Temp.
  - Lattice expansion
    - Delamination/cracking
  - Elastic Modulus and Fracture Toughness
    - Mechanical failure
- Validated mechanical property aspects of model
  - Elastic modulus as a function of P_{O2} predicted by theoretical modeling.
- Models based on fundamental thermodynamic laws and constants
  - ***Can be applied to any material set and geometry***